

Alleviating mass transfer limitations in industrial external-loop syngas-to-ethanol fermentation

Puiman, Lars; Abrahamson, Britt; Lans, Rob G.J.M.van der; Haringa, Cees; Noorman, Henk J.; Picioreanu, Cristian

DOI

[10.1016/j.ces.2022.117770](https://doi.org/10.1016/j.ces.2022.117770)

Publication date

2022

Document Version

Final published version

Published in

Chemical Engineering Science

Citation (APA)

Puiman, L., Abrahamson, B., Lans, R. G. J. M. V. D., Haringa, C., Noorman, H. J., & Picioreanu, C. (2022). Alleviating mass transfer limitations in industrial external-loop syngas-to-ethanol fermentation. *Chemical Engineering Science*, 259, Article 117770. <https://doi.org/10.1016/j.ces.2022.117770>

Important note

To cite this publication, please use the final published version (if applicable). Please check the document version above.

Copyright

Other than for strictly personal use, it is not permitted to download, forward or distribute the text or part of it, without the consent of the author(s) and/or copyright holder(s), unless the work is under an open content license such as Creative Commons.

Takedown policy

Please contact us and provide details if you believe this document breaches copyrights. We will remove access to the work immediately and investigate your claim.



Alleviating mass transfer limitations in industrial external-loop syngas-to-ethanol fermentation



Lars Puiman^{a,*}, Britt Abrahamson^b, Rob G.J.M. van der Lans^a, Cees Haringa^a, Henk J. Noorman^{a,c}, Cristian Picioreanu^d

^a Department of Biotechnology, Delft University of Technology, Delft, the Netherlands

^b Department of Civil and Environmental Engineering, University of Washington, Seattle, WA, USA

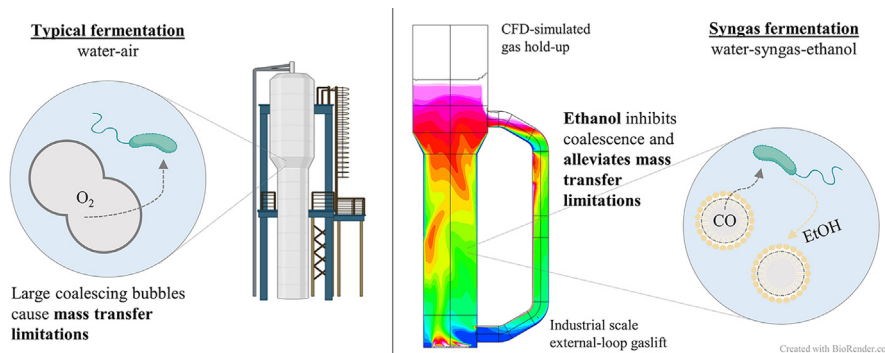
^c Royal DSM, Delft, the Netherlands

^d Biological and Environmental Sciences and Engineering Division, King Abdullah University of Science and Technology, Thuwal, Saudi Arabia

HIGHLIGHTS

- Detailed analysis on gas transfer rate in industrial syngas fermentation.
- CFD reveals mass transfer limitation topography in external-loop gas-lift reactors.
- Bubbles smaller than 2 mm are key to reach required mass transfer capacities.
- The produced ethanol minimizes bubble size and increases gas hold-up.
- Transport limitations in air–water systems can be alleviated in syngas fermentation.

GRAPHICAL ABSTRACT



ARTICLE INFO

Article history:

Received 8 February 2022

Received in revised form 13 May 2022

Accepted 22 May 2022

Available online 26 May 2022

Keywords:

Mass transfer

CFD

Airlift bioreactor

Ethanol

Syngas fermentation

Industrial

ABSTRACT

Mass transfer limitations in syngas fermentation processes are mostly attributed to poor solubility of CO and H₂ in water. Despite these assumed limitations, a syngas fermentation process has recently been commercialized. Using large-scale external-loop gas-lift reactors (EL-GLR), CO-rich off-gases are converted into ethanol, with high mass transfer performance (7–8.5 g.L⁻¹.h⁻¹). However, when applying established mass transfer correlations, a much poorer performance is predicted (0.3–2.7 g.L⁻¹.h⁻¹). We developed a CFD model, validated on pilot-scale data, to provide detailed insights on hydrodynamics and mass transfer in a large-scale EL-GLR. As produced ethanol could increase gas hold-up (+30%) and decrease the bubble diameter (≤2 mm) compared to air–water mixtures, we found with our model that a high volumetric mass transfer coefficient (650–750 h⁻¹) and mass transfer capacity (7.5–8 g.L⁻¹.h⁻¹) for CO are feasible. Thus, the typical mass transfer limitations encountered in air–water systems can be alleviated in the syngas-to-ethanol fermentation process.

© 2022 The Authors. Published by Elsevier Ltd. This is an open access article under the CC BY license (<http://creativecommons.org/licenses/by/4.0/>).

Abbreviations: EL, external-loop; ALR, airlift reactor; GLR, gas-lift reactor; MTC, mass transfer capacity.

* Corresponding author at: Delft University of Technology, Faculty of Applied Sciences, Department of Biotechnology, Van der Maasweg 9, 2629 HZ, Delft, The Netherlands.

E-mail address: L.Puiman@tudelft.nl (L. Puiman).

<https://doi.org/10.1016/j.ces.2022.117770>

0009-2509/© 2022 The Authors. Published by Elsevier Ltd.

This is an open access article under the CC BY license (<http://creativecommons.org/licenses/by/4.0/>).

1. Introduction

The conversion of waste gases by synthesis gas (syngas) fermentation has advanced to industrial scale in the last decade. In this process, a gas mixture containing CO, CO₂ and H₂ can be

Nomenclature

Latin

a	Specific surface area (m^{-1})
A	Area (m^2)
c	Concentration ($\text{kg}\cdot\text{m}^{-3}$)
D	Diameter (m)
D_{ax}	Axial dispersion ($\text{m}^2\cdot\text{s}^{-1}$)
D_L	Diffusion coefficient in liquid phase ($\text{m}^2\cdot\text{s}^{-1}$)
d_{32}	Sauter mean bubble diameter (m)
d_b	Bubble diameter (m)
g	Gravitational acceleration ($\text{m}\cdot\text{s}^{-2}$)
H	Henry coefficient ($\text{kg}\cdot\text{m}^{-3}\cdot\text{Pa}^{-1}$)
h	Height (m)
I	Turbulence intensity (%)
k	Turbulent kinetic energy ($\text{m}^2\cdot\text{s}^{-2}$)
k_L	Liquid-side mass transfer coefficient ($\text{m}\cdot\text{s}^{-1}$)
$k_L a$	Volumetric mass transfer coefficient (h^{-1})
L	Length (m)
MTC	Mass transfer capacity ($\text{g}\cdot\text{L}^{-1}\cdot\text{h}^{-1}$)
p	Pressure (Pa)
P	Power (W)
r	Radial position (m)
R	Radius (m)
t	Time (s)
T	Temperature (K)
u	Velocity ($\text{m}\cdot\text{s}^{-1}$)
\vec{u}	Velocity magnitude ($\text{m}\cdot\text{s}^{-1}$)
V	Volume (m^3)
v_{slip}	Slip velocity ($\text{m}\cdot\text{s}^{-1}$)
v_b^∞	Bubble rise velocity ($\text{m}\cdot\text{s}^{-1}$)
y	Mole fraction ($\text{mol}\cdot\text{mol}^{-1}$)
z	Axial position (m)

Greek

ε	Energy dissipation rate ($\text{m}^2\cdot\text{s}^{-3}$)
ε_G	Gas hold-up ($\text{m}_G^3\cdot\text{m}_D^{-3}$)
ε_L	Liquid hold-up ($\text{m}_L^3\cdot\text{m}_D^{-3}$)
η	Dynamic viscosity ($\text{kg}\cdot\text{m}^{-1}\cdot\text{s}^{-1}$)
θ	Circulation time (s)
ν	Kinematic viscosity ($\text{m}^2\cdot\text{s}^{-1}$)
ρ	Density ($\text{kg}\cdot\text{m}^{-3}$)
σ	Surface tension ($\text{N}\cdot\text{m}^{-1}$)

Sub- and superscripts

*	Saturation
∞	Final
ax	Axial
b	bubble
c	Circulation
con	Connector
e	exposure
d	Downcomer
D	Dispersion
G	Gas
in	Inlet
L	Liquid
r	Riser
s	Superficial
S	Solid
t	Tracer

converted by microbes (predominantly *Clostridium* spp.) into a range of chemicals, e.g. acetic acid, ethanol, acetone and isopropanol (Teixeira et al., 2018). The company LanzaTech has been able to commercialize the process of converting CO-rich off-gases from steel-mills into ethanol. Currently they deploy ethanol production facilities in China, while expanding their manufacturing network to other countries (Fackler et al., 2021; Köpke and Simpson, 2020; Teixeira et al., 2018).

Details of the full-scale operation are unknown in the scientific literature due to the proprietary nature of this process. It is expected that syngas conversion takes place in a gas-lift reactor with an external circulation loop (Li et al., 2017). This reactor configuration, also known as the external loop gas-lift reactor (EL-GLR) is like a conventional air-lift loop reactor as applied in waste-water treatment and industrial bioprocesses. Compared to the more established bubble column reactors (BCRs), in external-loop airlift reactors (EL-ALRs) there is forced liquid recirculation (potentially but not necessarily via pump action) through the downcomer (the external-loop), causing high liquid velocities, a more defined (plug)flow pattern and a shorter mixing time (Chisti and Moo-Young, 1987; Merchuk and Siegel, 1988). The external-loop might also be used for heat exchange, introduction of fresh feed and broth withdrawal (Jakobsen, 2014).

The increased liquid velocity in the riser is known to decrease the gas residence time and thus the gas hold-up (ε_G) and the volumetric mass transfer coefficient ($k_L a$) compared to a bubble column (Verlaan et al., 1989b; Weiland and Onken, 1981). At the same time, gas-liquid mass transfer is generally known to be one of the limiting factors in syngas fermentation processes (Asimakopoulos et al., 2018; Bredwell et al., 1999; Elisiário et al. (2021), Klasson et al., 1991, Yasin et al., 2015). For industrial etha-

nol production, it was determined that a $k_L a$ of at least 580 h^{-1} should be reached for commercial success (Köpke et al., 2011). Our preliminary calculations, based on publicly available data reported by LanzaTech, show that a mass transfer capacity (MTC) of 7 to 8.5 $\text{g}\cdot\text{L}^{-1}\cdot\text{h}^{-1}$ should be reached, which results in a $k_L a$ between 600 and 750 h^{-1} , based on a headspace pressure of 1 bar and 50% CO in the inlet gas (Figure S1).

For estimation of $k_L a$ in air-water systems, many relationships have been provided in the literature for different reactor types (Garcia-Ochoa and Gomez, 2009). With these relations the most likely $k_L a$ was estimated at industrial conditions and compared to the $k_L a$ from our preliminary calculations (Table 1), resulting into a MTC between 0.3 and 2.7 $\text{g}\cdot\text{L}^{-1}\cdot\text{h}^{-1}$. A clear discrepancy between the $k_L a$ obtained by these relations and the supposed industrial performance was found, as all engineering correlations predict a substantially lower $k_L a$. Although it is widely known that electrolytes, organic molecules (such as the produced ethanol), biomass, and the reactor geometry influence $k_L a$ (Garcia-Ochoa and Gomez, 2009; Heijnen and Van't Riet (1984)), the impact of these factors are not comprehensively considered with the correlations in Table 1. Furthermore, empirical relations obtained for ALRs were derived at smaller scales and their validity for larger scales bears uncertainties. The non-standard reactor geometry and irregular flow pattern in industrial reactors complicate the prediction of the mass transfer performance using common correlations, which are normally valid for a narrow range of conditions and were derived in shorter columns (influencing $u_{G,s}$) while assuming ideal mixing. Spatio-temporal variations complicate the *a priori* estimation of ε_G , $k_L a$ and MTC as particular geometry configurations strongly influence the hydrodynamics in ALRs (e.g. riser width/height, separator dimensions and the particular connection of the

Table 1

Relationships used for the prediction of $k_L a$ in Newtonian media in a large-scale EL-GLR, as well as typical $k_L a$ values for industrial operation. See Table S2 and Table S3 for the meaning, units and calculation of variables in these equations. The empirical correlations were developed for air–water systems, and would require a small correction (around 5% lower) for CO due to its lower diffusion coefficient compared to oxygen (Van Hecke et al., 2019).

Reference	Equation	$k_L a$ (h^{-1})
LanzaTech estimation		600–750
Empirical correlations		
<i>External-loop airlift</i>		
Bello et al. (1985)	$k_L a = 0.76 \cdot \left(1 + \frac{A_d}{A_r}\right)^{-2} \cdot u_{G,S}^{0.8}$	~ 130
Chisti et al. (1986)	$k_L a = \varepsilon_L \left(1 + \frac{A_d}{A_r}\right)^{-1} u_{G,S}^{0.899} \cdot (0.349 - 0.102c_S)$	~ 40
Chisti and Moo-Young (1987)	$k_L a = 1.27 \cdot 10^{-4} \cdot \left(\frac{\rho_G}{\rho_L}\right)^{0.925}$	~ 75
<i>Bubble column</i>		
Deckwer et al. (1974)	$k_L a = 0.5 \cdot u_{G,S}^{0.884}$	~ 80
Deckwer et al. (1983)	$k_L a = 0.467 \cdot u_{G,S}^{0.82}$	~ 90
Jackson and Shen (1978)	$k_L a = 0.53 \cdot u_{G,S}^{1.15}$	~ 30
Heijnen and Van't Riet (1984)	$k_L a = 0.32 \cdot u_{G,S}^{0.7} \cdot 1.024^{(T-293)}$	~ 140
Dimensionless relations		
Akita and Yoshida (1973)	$(Sh)a \cdot D_r = 0.6Eo^{0.62} Ga^{0.3} Sc^{0.5} \varepsilon_G^{1.1}$	~ 170
Nakanoh and Yoshida (1980)	$(Sh)a \cdot D_r = 0.09Eo^{0.75} Ga^{0.4} Sc^{0.5} Fr^1$	~ 230
Kawase et al. (1987)	$(Sh)a \cdot D_r = 0.452Eo^{0.62} Ga^{0.3} Sc^{0.5} Fr^1 Re^1$	~ 15
Uchida et al. (1989)	$(Sh)a \cdot D_r = 0.17Eo^{0.62} Ga^{0.3} Sc^{0.5} \varepsilon_G^{1.1}$	~ 50
Vatai and Tekić (1989)	$(Sh)a \cdot D_r = 0.031Eo^{0.75} Ga^{0.4} Sc^{0.5} Fr^1$	~ 80
Kawase and Hashiguchi (1996)	$(Sh)a \cdot D_r = 0.142Eo^{0.6} Sc^{0.5} Fr^{0.075} Re^{0.875} \left(1 + \frac{A_d}{A_r}\right)^{-97/80}$	~ 170

downcomer). For example, while the liquid and gas velocities are expected to be high in the riser, these should decrease in the wider separator section in the top of the vessels and consequently increase the local ε_G (Hernández-Calderón et al., 2017).

Several models have been developed to describe hydrodynamics of pilot- and full-scale airlift bioreactors. The model by Van der Lans (1985) predicted the axial mean values of liquid circulation velocity and gas fraction in a pilot-scale external-loop bioreactor well. Van Benthum et al. (1999) modelled three-phase hydrodynamics (liquid velocity, gas and solid hold-up) in a biofilm airlift suspension extension reactor, wherein the liquid velocity in a gas-free downcomer is controlled independently from the gas flow velocity. While neglecting spatial variations of gas, liquid and solids concentrations in the internal regions, the model was well able to predict the pilot-scale hydrodynamics. Earlier, Heijnen et al. (1997) described the liquid circulation velocity and gas hold-up in an industrial-scale biofilm internal-loop airlift suspension reactor, based on mass and momentum balances. This model is applicable to three hydrodynamic regimes: gas-free downcomer (regime 1), entrained gas in downcomer (regime 2) and gas back-circulation via downcomer (regime 3). We argue that in the LanzaTech case, operation in regime 1 or 2 may be preferred compared to regime 3 as the latter could reduce the CO partial pressure and thus its saturation concentration in the riser.

Convection-dispersion and tanks-in-series (1D) models have been proposed to understand mixing and mass transfer phenom-

ena in small-scale airlift reactors (Znad et al., 2004), but it is unclear how the flow pattern deviates from these simple mixing models for the large-scale EL-GLR. It is generally known that large-scale BCRs show high axial dispersion coefficients (Heijnen and Van't Riet (1984)) but that EL-ALRs studied at lab and pilot-scale display more plug-flow behaviour (Verlaan et al., 1989b). As the axial dispersion behaviour is unclear in an industrial EL-GLR, the convection–dispersion models turned out to be unsuitable for the prediction of the large-scale flow pattern and gas–liquid mass transfer rates. Furthermore, several relations have been developed to describe the mass transfer coefficient k_L , based on local conditions such as the slip velocity and the eddy dissipation rate (Table 2). These relations require a high spatial resolution, which cannot be provided by the 0D and 1D models.

With 3D computational fluid dynamics (CFD) models a high spatio-temporal resolution can be obtained, albeit with a much greater computational effort than when applying simple mixing models. For EL-ALRs, several authors used CFD to study the hydrodynamics and the mixing behaviour (Karcz et al., 2013; Moudoud et al., 2018; Roy et al., 2006). Hydrodynamics and oxygen mass transfer in a lab-scale sectionalized EL-ALR has been studied recently; it was demonstrated that the $k_L a$ predicted with Equation 5 (Table 2) matched the experimental data better than predictions from Equation 1 and 3 (Teli and Mathpati, 2021). Similar work was done earlier, wherein it was observed that Equation 3 strikingly showed a good agreement with experimental results

Table 2

The different relations that are used for predicting the liquid-side mass transfer coefficient, k_L .

Number	Reference	Equation	
<i>Bubble-based models</i>			
(1)	Higbie (1935)	$k_L = 2\sqrt{\frac{D_{L,CO}}{\pi t_c}} = 2\sqrt{\frac{D_{L,CO} v_{slip}}{\pi d_b}}$	$d_b > 2$ mm (Heijnen and Van't Riet (1984))
(2)	Calderbank and Moo-Young (1961)	$k_L = 0.42 \left(\frac{\Delta \rho v_L g}{\rho_L}\right)^{\frac{1}{2}} \left(\frac{D_{L,CO}}{v_L}\right)^{\frac{1}{2}}$	Non-rigid bubbles
<i>Eddy-based models</i>			
(3)	Kaštanek (1977)	$k_L = 2\sqrt{\frac{D_{L,CO}}{\pi t_c}} = 1.13 D_{L,CO}^{\frac{1}{2}} (\varepsilon/v_L)^{\frac{1}{4}}$	Theoretical
(4)	Linek et al. (2005)	$k_L = 0.45 D_{L,CO}^{\frac{1}{2}} (\varepsilon/v_L)^{\frac{1}{4}}$	Empirical
(5)	Lamont and Scott (1970)	$k_L = 0.4 D_{L,CO}^{\frac{1}{2}} (\varepsilon/v_L)^{\frac{1}{4}}$	Empirical
(6)	Kawase and Moo-Young (1990)	$k_L = 0.3 D_{L,CO}^{\frac{1}{2}} (\varepsilon/v_L)^{\frac{1}{4}}$	Empirical

(Dhanasekharan et al., 2005). Most of these models were developed for lab and pilot-scale EL-ALRs, with riser diameters smaller than 0.14 m, where wall effects can be significant (Chisti and Moo-Young, 1987).

A CFD model for syngas fermentation in a BCR with a population balance model for the gas phase was developed recently (Siebler et al., 2019). Low $k_L a$ values and thus low CO transfer rates, low dissolved CO concentrations and low CO uptake rates were obtained as >50% of the bubbles had a relatively high bubble diameter ($d_b > 8$ -mm). Several one-dimensional (1D) models have been presented for syngas fermentation in large-scale BCRs as well. De Medeiros et al. (2020) developed such a model for the optimization of different process conditions. They determined that strategies needed to be obtained to enhance the $k_L a$ with at least a factor three, relative to air–water correlations, to decrease the minimum ethanol selling price to \$0.7/L and reach high (70%) thermodynamic efficiency. Another BCR model was coupled with a black-box stoichiometric model for *C. autoethanogenum* based on thermodynamics in order to estimate the ethanol productivity in such a reactor. High productivities were obtained ($4.25 \text{ g}_{\text{EtOH}} \cdot \text{L}^{-1} \cdot \text{h}^{-1}$), but this was at the expense of the gas utilization (only 17%) as high gas flow rates were used (Benalcázar et al., 2020). In another 1D model, with kinetics reported by LanzaTech, a genome-scale metabolic model for a proprietary *C. autoethanogenum* strain was coupled to bubble column hydrodynamics. In their model $k_L a$ and microbial CO uptake rate varied axially between 350 and 425 h^{-1} and 0 and $7 \text{ g} \cdot \text{L}^{-1} \cdot \text{h}^{-1}$, respectively, by assuming d_b below 1.5 mm and constant k_L of $1 \cdot 10^{-4} \text{ m} \cdot \text{s}^{-1}$ (Li et al., 2019). However, detailed analyses how the low d_b and high MTC could be accomplished in industrial reactors are lacking.

Thus far, no CFD model has been developed for describing the hydrodynamics and CO mass transfer in a large-scale external-loop gas–liquid reactor, for studying the required conditions to minimize the gas–liquid mass transfer limitations in an industrial syngas fermentation process. Next to that, the results of such a model would provide information to be used for subsequent reactor design and optimization. The model that we have developed in this study for hydrodynamics and mass transfer in an EL-ALR was first tested and validated by comparing local axial gas and liquid flow velocities in the riser and the downcomer, gas hold-up, and turbulence intensity with pilot-scale results obtained by Young et al. (1991). Then, using the same model equations, the large-scale EL-GLR hydrodynamics and gas transfer were simulated and compared with correlations and observations from literature. For varying bubble diameters (between 1 and 7 mm), higher temperatures and gas hold-up, and a range of headspace pressures, $k_L a$ and MTC were determined using different relations (Table 2), in order to establish the best operation window for high industrial performance.

2. Methods

2.1. Reactor geometry and mesh

In this work, two reactor geometries were considered: A pilot-scale geometry to compare CFD model predictions with experimental results and a full-scale reactor for the subsequent mass transfer study. The hydrodynamic CFD model was applied to data obtained by Young et al. (1991) for a pilot-scale external-loop reactor (2.95 m high, riser and downcomer diameter of 19 and 14 cm, 260 L reactor volume, 160 L liquid volume). This reactor configuration was chosen as it was found that the gas hold-up was independent of the riser diameter when wider than 14 cm (Chisti and Moo-Young, 1987). The 3D geometry was developed using ANSYS Design Modeller. A polyhedral mesh (400000 cells, 0.27 minimum

orthogonal quality) with a higher resolution in the dispersed-phase domain was developed in ANSYS Meshing (Figure S2).

The dimensions of the industrial-scale reactor were estimated from openly available pictures of the Shougang-LanzaTech plant, and are schematically represented in Fig. 1. The 3D geometry has been developed using cylindrical bodies, with a ring sparger (Young et al., 1991) mounted at 0.1 m above the reactor base. The total volume of the reactor equals 840 m^3 , with an ungasged liquid volume of 565 m^3 , which roughly corresponds to the 500 m^3 volume presented by LanzaTech (Fackler et al., 2021). A mesh with 370,000 polyhedral cells, 0.3 minimum orthogonal quality, 20 cm cell size and three refined boundary layers near all walls (including sparger), was constructed in Fluent Meshing. A mesh refinement study done using meshes with 1.6 and 1.9 million cells established that the 370000-cell mesh was sufficient for determining $k_L a$ and MTC within 10% accuracy (Figure S2, Table S3).

2.2. Fluid dynamic model

The transient gas–liquid flow was computed within ANSYS Fluent 2020R1 with the Eulerian multiphase flow model, with implicit volume fraction formulation, dispersed RNG k - ϵ turbulence model, which is the recommended choice for bubble column modelling (Laborde-Boutet et al., 2009), and standard wall functions. The forces involved in the two-phase interaction were surface tension (continuum surface force), drag (Fluent's universal-drag model) and gravity. A model with a similar set of forces was used before for syngas fermentation modelling in BCRs (Siebler et al., 2019).

In the pilot-scale ALR, mean air bubble diameters ranged from 4 to 6 mm (Young et al., 1991), therefore as dispersed phase 5 mm bubbles were modelled. For the large-scale reactor, the mean bubble diameter is unknown and could range between 1 and 7 mm, based on the liquid properties and operating conditions (Heijnen and Van't Riet (1984)). Because coalescence inhibition can be expected due to the salt and ethanol-rich fermentation broth, 3 mm bubbles were modelled in the large-scale hydrodynamic model, according to Krevelen and Hoftijzer (1950), by assuming a sparger orifice size of 0.75 mm.

A mass–flow inlet was used on the sparger surface at the bottom of the reactor, providing a fixed mass flow rate of gas (Table 3). A pressure-outlet with gas backflow was assumed at the top of the column, with the headspace pressure of 101 kPa in both reactors. Sensitivity analyses were done with 304 kPa and 608 kPa headspace pressure for the large-scale reactor. Boundary conditions considered a turbulence intensity of 5% and the local vessel diameter. To all the walls standard no-slip conditions were assigned.

As the precise liquid medium properties are unknown due to the presence of variable concentrations of cells and ethanol, the properties of water at 25 °C were assumed for the liquid phase (Table 4). Gas density differences were accounted for using the ideal gas law. Both reactor models contained a gas headspace, by initializing the headspace gas fraction to be 1.

2.3. Mass transfer

The mass transfer studies in the large-scale bioreactor were performed after a statistically stationary (“steady”) flow field was established (after 1000 s simulation time, using 3 mm bubbles). For an additional 200 s, dynamic flow data was exported every second for time-averaging and processed in Tecplot 360 EX 2018 R1. Based on the computed flow field, $k_L a$ and MTC were calculated via six different relations for k_L (Table 2). Spherical bubbles were assumed because of the small bubble diameter and bubble-stabilizing effects of dissolved solutes (Equation (7)) as well as a linear gradient in axial gas phase CO mole fraction y_{CO} (considering 90% CO conversion (Figure S1)) (Equation (8)). The impact of the

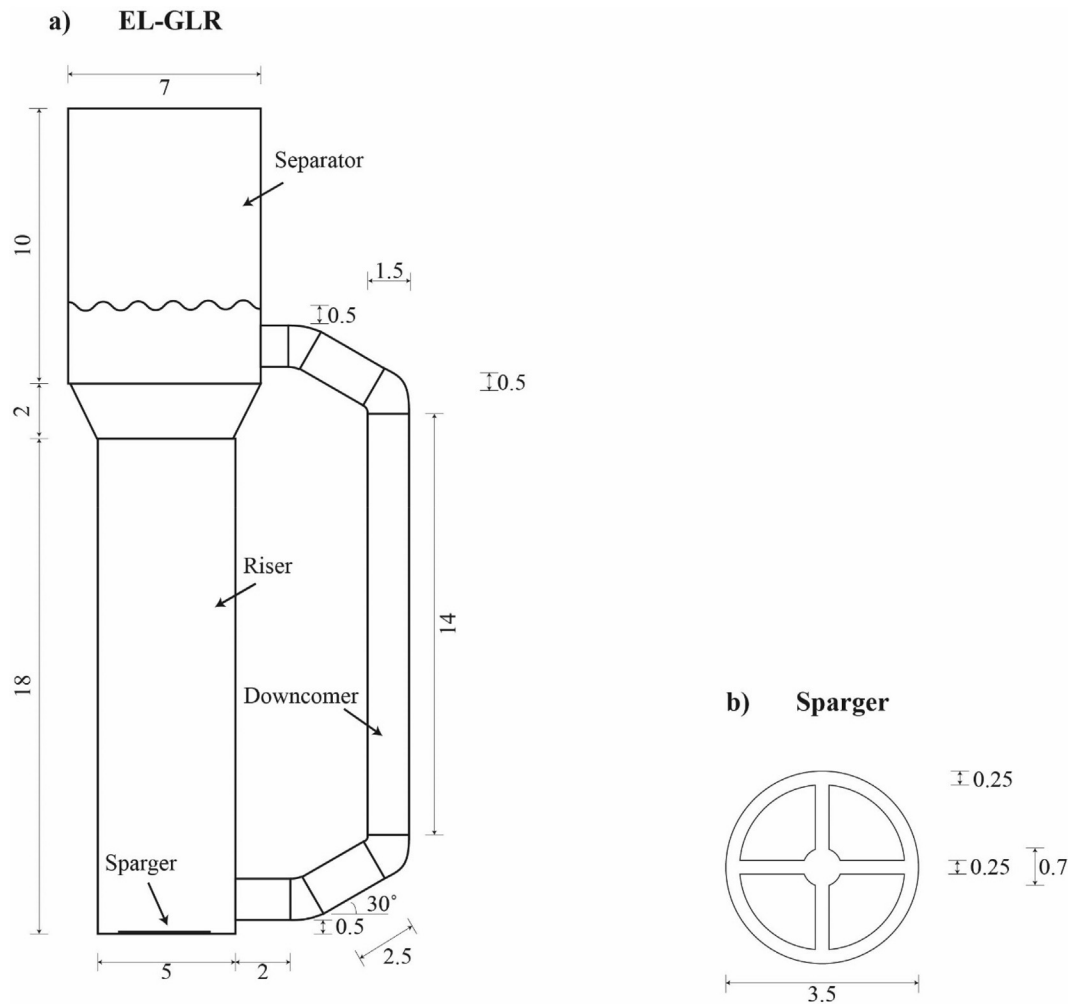


Fig. 1. Schematic representation of a) the industrial-scale external-loop gas-lift reactor and b) the sparger geometry. The wavy line represents the initial (ungassed) liquid height. All dimensions are in meters.

Table 3

Values used for the mass flow inlet boundary condition in the various models. The superficial gas velocity was calculated by determining the gas flow rate ($\text{m}^3 \cdot \text{s}^{-1}$) using the local pressure at the sparger (Table S1). For scale comparison, the gas mass flow per volume liquid is provided.

Superficial gas-velocity ($\text{cm} \cdot \text{s}^{-1}$)	Mass flow per volume liquid ($\text{kg} \cdot \text{m}^{-3} \cdot \text{s}^{-1}$)	Mass flow inlet ($\text{kg} \cdot \text{s}^{-1}$)
Pilot-scale reactor		
0.96	$2.37 \cdot 10^{-3}$	$3.96 \cdot 10^{-4}$
2.1	$5.19 \cdot 10^{-3}$	$8.66 \cdot 10^{-4}$
4.7	$1.14 \cdot 10^{-2}$	$1.90 \cdot 10^{-3}$
8.4	$2.04 \cdot 10^{-2}$	$3.4 \cdot 10^{-3}$
Industrial-scale reactor		
2.8	$3.73 \cdot 10^{-3}$	2.11

bubble size was studied in the 1–7 mm range. The influence of the operating temperature was considered as it affects the liquid viscosity, CO diffusion coefficient and Henry constant (Table 5). For the calculation of MTC, microbial CO uptake kinetics are not required, instead a dissolved CO concentration of $0 \text{ g} \cdot \text{L}^{-1}$ was assumed in all grid cells.

$$MTC = k_L a \cdot c_{L,CO}^* = k_L \cdot \frac{6\epsilon_G}{d_b \epsilon_L} \cdot H_{CO} p y_{CO} \quad (7)$$

$$y_{CO}(z) = -\frac{(y_{CO,in} - 0.9y_{CO,in})^3}{h_D} z + y_{CO,in} \quad (8)$$

2.4. Model solution

The transient models were solved using ANSYS Fluent 2020R1. For the pilot-scale models, a time step of 0.01 s was used with a maximum of 30 iterations per time step, wherein the residuals decreased to $O(10^{-3})$. The results presented here were obtained by storing flow data at the positions mentioned by Young et al. (1991) every 0.01 s, starting at 50 s (when a steady flow field was reached) until 110 s flow time.

For the industrial reactor, the time step dt was gradually increased from an initial 0.01 s until 0.65 s, $dt = 0.025$ s until 3 s, $dt = 0.05$ s until 5 s and $dt = 0.1$ s from 5 s on. This time-stepping strategy was required to keep solution convergence (residuals $< O(10^{-3})$) within 10–25 iterations per time step, and found to be crucial to achieving convergence near the mesh-refined sparger location. The solution methods, spatial discretization and relaxation factors for both reactor models are given in Table S4.

3. Results and discussion

In this section, the flow pattern predicted by the CFD model will first be compared with the pilot-scale data obtained by Young et al. (1991) (section 3.1). After this, the results at the large-scale are discussed (section 3.2) in terms of the gas hold-up, flow pattern and hydrodynamic regime. Then, results on mass transfer and strategies for relieving the gas-liquid mass transfer limitations will be

Table 4
Parameters used in the CFD models.

Symbol	Description	Pilot-scale	Industrial-scale	Unit
g	Gravitational acceleration	-9.81	-9.81	m.s^{-2}
T	Temperature	293.15	310.15	K
p_0	Operating pressure	101,325	101,325	Pa
d_b	Bubble diameter	$5 \cdot 10^{-3}$	$3 \cdot 10^{-3}$	m
σ	Surface tension	0.072	0.072	N.m^{-1}
Gas phase				
ρ_G	Gas density	Ideal gas law	Ideal gas law	kg.m^{-3}
η_G	Gas viscosity	$1.78 \cdot 10^{-5}$	$1.72 \cdot 10^{-5}$	$\text{kg.m}^{-1}.\text{s}^{-1}$
$y_{\text{CO},\text{in}}$	Inlet mole fraction	-	0.5	$\text{mol}_{\text{CO}}.\text{mol}_{\text{C}}^{-1}$
Liquid phase				
ρ_L	Water density	998	998	kg.m^{-3}
η_L	Liquid viscosity	$1.0 \cdot 10^{-3}$	$1.0 \cdot 10^{-3}$	$\text{kg.m}^{-1}.\text{s}^{-1}$

Table 5
Parameters used for mass transfer calculations.

Symbol	Description	20 °C	37 °C	Unit	Source
ν_L	Kinematic viscosity	$1.018 \cdot 10^{-6}$	$7.121 \cdot 10^{-7}$	$\text{m}^2.\text{s}^{-1}$	Reid et al. (1987)
$D_{\text{L,CO}}$	CO diffusion coefficient	$1.78 \cdot 10^{-9}$	$2.71 \cdot 10^{-9}$	$\text{m}^2.\text{s}^{-1}$	Cussler (2011)
H_{CO}	Henry coefficient	$2.93 \cdot 10^{-7}$	$2.29 \cdot 10^{-7}$	$\text{kg.m}^{-3}.\text{Pa}^{-1}$	Sander (2015)

discussed (section 3.3), before we sketch the implications of this research in the outlook (section 3.4).

3.1. Pilot-scale flow pattern

The computed liquid velocity in the riser was compared with the velocity profiles along the radius obtained experimentally

by Young et al. (1991) (Fig. 2). The computed mean liquid velocity in the riser approximates the measured one with maximum deviations of 36% (Table S5). However, the computed velocity gradients along the column radius were consistently smaller (i.e. flatter velocity profiles) than those measured (i.e. showing usually a sharp maximum at the axis at $r/R = 0$). The radial profiles of the turbulence intensities in both the riser and downcomer are quite

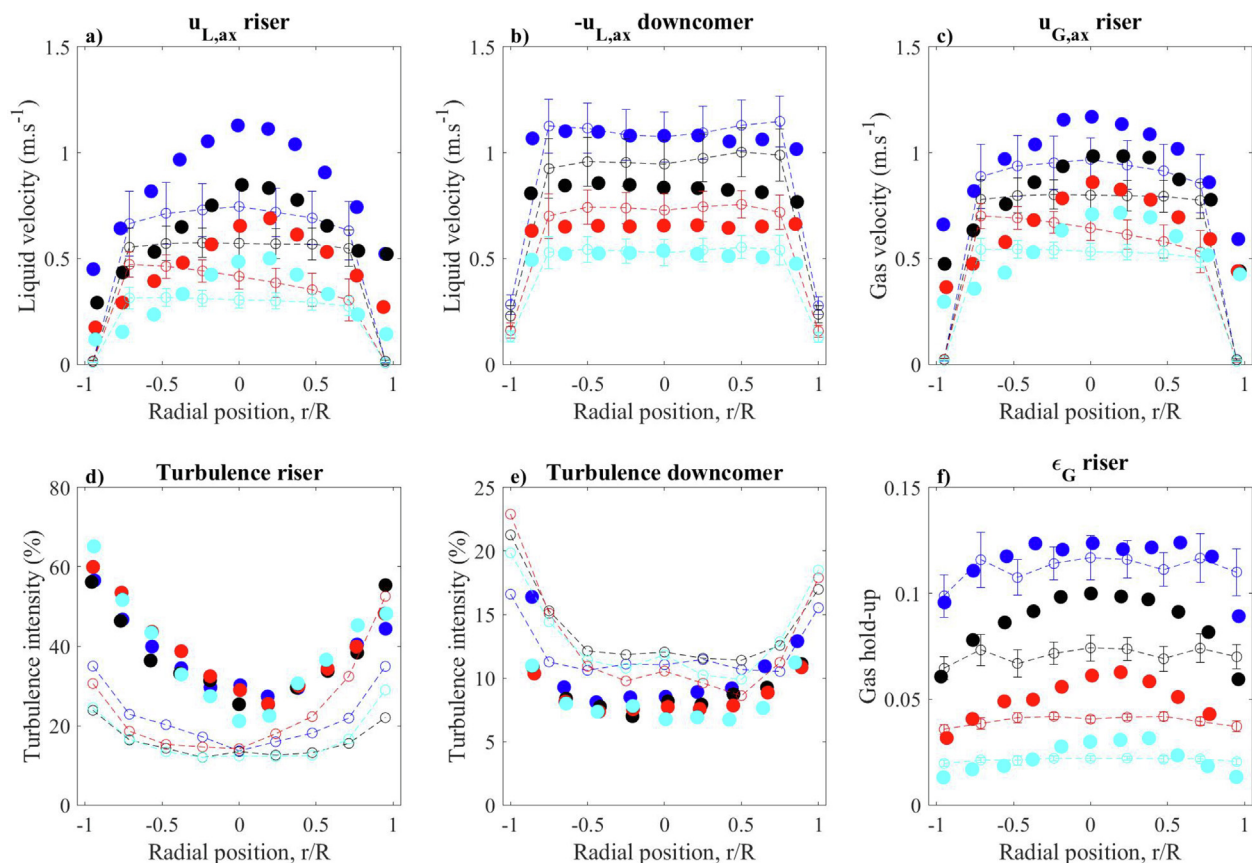


Fig. 2. Comparison of radial profiles obtained by experiments in a pilot-scale EL-ALR (Young et al., 1991) (filled circles) and mean values of CFD results (open circles with dashed lines) for different $u_{G,s}$ (8.4 (blue), 4.7 (black), 2.1 (red) and 0.96 cm.s^{-1} (cyan)). a) the axial liquid velocity in the riser ($u_{L,ax}$), b) the axial liquid velocity in the downcomer ($-u_{L,ax}$), c) the axial gas velocity in the riser ($u_{G,ax}$), d) the turbulence intensity in the liquid in the riser and e) downcomer, and f) the gas hold-up in the riser. Error bars: the standard deviation of the CFD results during 60 s simulation time (data stored every 0.01 s).

similar to the data, but the model underestimates the turbulence intensity in the riser, while overestimating in the downcomer. This is probably a result of the simplified set of forces considered in the model. Roy et al. (2006) were able to model the radial liquid velocity profile by using the standard $k-\epsilon$ model and taking the turbulence dispersion and lift forces into account, together with a conveniently chosen bubble size. On the other hand, liquid velocity measurement errors up to 10% for the riser were noted from a liquid phase mass balance by Young et al. (1991), which could possibly explain part of the deviation between model and measurements. The (gas-free) downcomer velocity profile, however, showed good correspondence, as well as the profiles predicted for the gas hold-up and gas velocity. The trends for increasing superficial gas velocities were modelled correctly for all variables.

Furthermore, by simulated injection of a liquid tracer (with the same properties as water) just above the sparger, it was determined that the model can predict the typical circulating liquid mixing behaviour as often shown in airlift reactors (Chisti and Moo-Young, 1987; Voncken et al., 1964). The tracer concentration profile over time c_t extracted from the CFD simulations was normalized with the final (steady state) concentration $c_{t,\infty}$. This normalized tracer concentration over time (t) was fitted with Equation (9) (Chisti and Moo-Young, 1987) expressing the fluctuations of concentration over a normalized time θ ($\theta = t/t_c$, with t_c the circulation time), as function of the Bodenstein number ($Bo = u_{L,ax}L_c/D_{ax}$, with L_c the circulation length and D_{ax} the axial dispersion coefficient).

$$\frac{c_t}{c_{t,\infty}} = \left(\frac{Bo}{4\pi\theta}\right)^{1/2} \sum_{n=1}^{\infty} \exp\left[-\frac{(n-\theta)^2 Bo}{4\theta}\right] \quad (9)$$

In this way, Bo and t_c for the EL-ALR were determined at several locations in the reactor (Fig. 3). The model predicted Bo values around 45, which are typical estimations for Bo in an ALR (Verlaan et al., 1989c, Verlaan et al. 1989a), indicating the dominance of the plug-flow in the reactor. A mean circulation time of about 7.6 s resulted from the tracer model with a $u_{G,s}$ of $8.4 \text{ cm}\cdot\text{s}^{-1}$.

Considering that most of the flow parameters were determined to be within a 25% range of experimental values (Table S5) and the good correspondence with mixing theory, we considered the model appropriate for engineering calculations. Furthermore, the most important variable concerning mass transfer, the gas hold-up, was reasonably well predicted. In order to be sure that the radial liquid velocity profile is properly predicted it will be compared with theoretical predictions for this profile in large-scale EL-ALRs in the upcoming section.

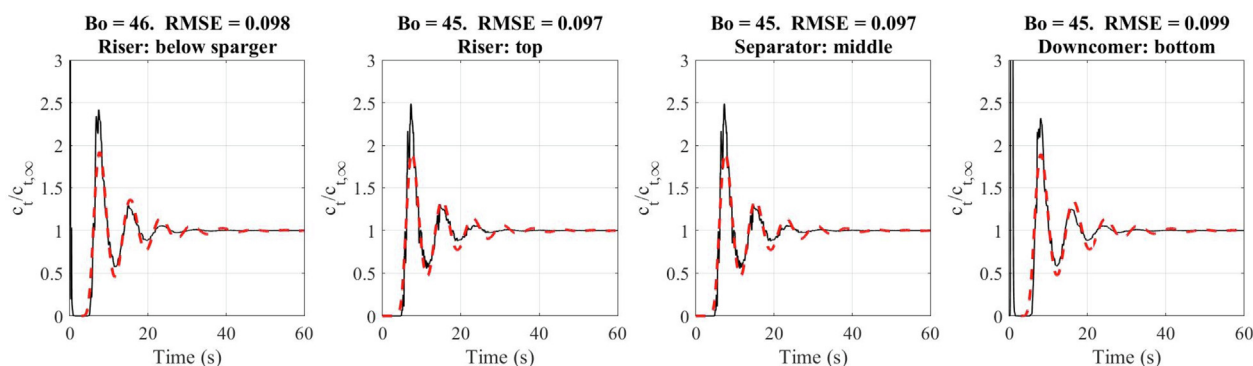


Fig. 3. The normalized concentration of a tracer obtained from the CFD model (black lines) and concentration according to the axial dispersion model for ALR (Eq. (9)) (red lines), compared at four locations in the pilot-scale reactor. For all locations, the Bodenstein number was ~ 45 with the root-mean-square-error (RMSE) smaller than 0.1. The CFD data have been obtained at $u_{G,s}$ of $8.4 \text{ cm}\cdot\text{s}^{-1}$.

3.2. Large-scale flow pattern

In this section, the results of the large-scale reactor CFD model are presented. First, its ability to predict the gas fraction is discussed, since this is a key variable regarding mass transfer. Then the gas and liquid velocity-fields are analysed in detail. Lastly, the radial profiles of the liquid velocity in the riser and the observed time-variations are discussed.

The simulated gas hold-up in the EL-GLR was on average 0.13 at a superficial gas velocity of $2.8 \text{ cm}\cdot\text{s}^{-1}$. This value was in good agreement with the values obtained from several correlations available in literature for BCRs and EL-ALRs (Table 6).

The local values of the instantaneous gas hold-up (Fig. 4a) were averaged in time over 200 s (Fig. 4c). The CFD simulations indicate that at the bottom of the reactor, the freshly sparged gas is strongly pushed towards the wall of the riser, which might result in bubble coalescence, by the liquid exiting the downcomer. This is also visible in the liquid flow patterns (Fig. 4b, d). When the gas is pushed towards the left side, the local liquid velocity increases, creating a circulation loop around the downcomer outlet. Similar behaviour has been observed experimentally for bottom-plate spargers (Chisti and Moo-Young, 1987) and also from CFD models developed for different EL-ALRs (Roy et al., 2006).

Halfway the riser the instantaneous gas hold-up shows an asymmetric distribution (Fig. 4a), while the time-averaged gas hold-up (Fig. 4c) is more symmetrical with high values along the riser axis, indicating an oscillating gas plume. This is also apparent from the velocity plots, with liquid moving back and forth between the sides (Fig. 4b). Such oscillating behaviour has been observed experimentally in internal-loop airlift reactors (Ziegenhein et al., 2016). However, by time-averaging these movements cancelled-out and a quasi-symmetric velocity profile was obtained (Fig. 4d). While the liquid mostly rises, the negative values observed near the riser wall indicate a certain degree of backmixing, which has also been observed experimentally in ALRs (Merchuk and Siegel, 1988; Zhang et al., 2019). This internal liquid recirculation contributes to the overall mixing in the riser and creates axial and radial dispersion.

Approaching the gas-liquid separator at the top of the riser, the gas hold-up tends to increase as gas expansion (decreasing hydrostatic pressure) and the wider separator diameter (decreasing the local liquid velocity) increase the gas residence time. This particular section of the reactor could become advantageous for mass transfer because the expected lower CO saturation concentration (due to the lower hydrostatic pressure and a lower CO fraction in the gas) can be compensated by the increase in gas hold-up.

Just above and in the downcomer inlet, high gas hold-ups as well as high liquid flow velocities were predicted. While the liquid

Table 6

The 200 s time- and volume-averaged gas hold-up determined by CFD in the EL-GLR, riser and downcomer, compared with values from established correlations. The values of $u_{G,S,r}$ and $u_{L,S,r}$ used in the correlations were the averages of the time-averaged axial superficial velocities computed in six horizontal planes across the riser.

Study	Reactor type	Equation	Gas hold-up
This study	EL-GLR	3D CFD model	0.126
Zuber and Findlay (1965) ¹	BCR	$\varepsilon_{G,r} = \frac{u_{G,S,r}}{1.08(u_{G,S,r} + u_{L,S,r}) + v_b^\infty}$	0.137
Heijnen and Van't Riet (1984) ¹	BCR (homogeneous flow regime)	$\varepsilon_{G,r} = \frac{u_{G,S}}{v_b^\infty}$	0.112
Chisti and Moo-Young, 1987	EL-ALR	$\varepsilon_{G,r} = \frac{u_{G,S,r}}{0.24 + 1.35(u_{G,S,r} + u_{L,S,r})^{0.93}}$	0.124
Bello et al. (1985)	EL-ALR	$\varepsilon_G = 0.16 \left(\frac{u_{G,S,r}}{u_{L,S,r}} \right)^{0.56} \left(1 + \frac{A_d}{A_r} \right)^{-1}$	0.149
Choi and Lee (1993) ²	EL-ALR	$\varepsilon_{G,r} = 0.288 u_{G,S,r}^{0.504} \left(\frac{A_d}{A_r} \right)^{-0.098} \left(\frac{L_{con}}{L_d} \right)^{-0.094}$	0.112

1: $v_b^\infty = 0.25$ m/s, 2: $L_{con} = 0.5$ m and $L_d = 19.5$ m. Other parameters given in Table S1.

flow is directed horizontally and downwards, the bubbles dragged into the downcomer will rise. This causes a sharp separation between gas and liquid and consequently high gas hold-ups. Similar behaviour was found by modelling EL-ALRs with comparable geometry (Dhanasekharan et al., 2005; Karcz et al., 2013; Moudoud et al., 2018). Degassing geometries might prevent the gas to flow into the downcomer (Heijnen et al., 1991). At the left side of the downcomer, the drag by the liquid and buoyancy of the gas bubbles are in equilibrium and therefore a stable gas hold-up is obtained over time (Fig. 4c). This corresponds to the second gas entrainment regime (Heijnen et al., 1997), wherein the gas bubbles entrained in the downcomer do not reach the bottom and only partially fill the downcomer. Higher local gas hold-up in the downcomer close to the riser wall was also observed in internal-loop airlift reactors (Choi and Lee, 1990).

The question emerges on how high the recirculation through the downcomer is in the EL-GLR compared with the internal recirculation in the riser. From the velocity field it was determined that, in this particular reactor geometry, about 14% of the liquid goes down via the downcomer and flows downwards near the riser walls. This indicates that axial mixing in the riser is significant and plug-flow behaviour cannot be assumed for the liquid phase. Although the downcomer appears to be poorly used for the liquid circulation in the studied operation regime, it clearly increases the liquid flowrates in the riser compared to a bubble column (with zero net axial liquid velocity). Such results highlight the added value of CFD predictions as this behaviour could not be predicted with simpler (1D) models.

In the pilot-scale model, a parabolic velocity profile was not observed (Fig. 2) and further radial liquid flow was not determined, therefore the large-scale model needed to simulate local axial and radial velocity variations. At several heights in the riser, the profile of axial liquid velocity along the whole riser diameter was calculated over time, then compared with a parabolic profile (Equation (10), Fig. 5) characteristic for BCRs and ALRs (Menzel et al., 1985). Both parameters of the parabolic profiles, velocity at the riser axis $u_{L,ax}(r = 0)$ and superficial liquid velocity $u_{L,S,ax}$, were taken from time-averaged CFD results.

$$u_{L,ax}(r) = (u_{L,ax}(r = 0) - u_{L,S,ax}) \left(1 - 2 \left(\frac{r}{R} \right)^2 \right) + u_{L,S,ax} \quad (10)$$

At the lower locations (5.1 m and 7.4 m) the liquid velocity profile is skewed towards the left side, due to the liquid entering from the downcomer. However, the liquid velocity profile shifts towards the central axis at higher locations in the riser, where it matches the proposed parabolic profile. It should be noted that there are large time-variations, which should be taken into account when analysing mass transfer in EL-GLRs, for example by time-averaging for 200 s (Figure S3).

Many phenomena found at pilot-scale were also predicted by the simulations to occur in the large-scale external-loop reactor. Moreover, the predicted overall gas hold-up and liquid flow velocities showed a good match with literature relations. From all these indicators it can be concluded that with a CFD model the large-scale behaviour can be described properly. With this hydrodynamic model, subsequent calculations on $k_L a$ and MTC will be performed and are discussed in the next section.

3.3. Mass transfer

Syngas fermentation processes are developed towards a multitude of products, e.g. acids (acetic acid), alcohols (ethanol, propanol, butanol), ketones (acetone), glycols (2,3-butanediol), aromatics, dienes, esters and terpenes (Köpke and Simpson, 2020). Although the literature is very scarce on their influence on mass transfer in fermentation broths, it is known that the hydrophilic products inhibit bubble coalescence in water, thereby decreasing the Sauter mean bubble diameter (d_{32}) (Keitel and Onken, 1982), and increasing $k_L a$ (Zlokarnik, 1980). In a pilot-scale bubble column (3 m high, 20 cm width), Keitel and Onken (1982) found decreases in d_{32} from 4 to 1 mm and doubling of ε_G from 2 to 4%, for a variety of alcohols. By increasing hydrophobic chain length, stronger effects (i.e. occurring at lower concentrations) were reported, for d_{32} , ε_G , and $k_L a$ (Keitel and Onken, 1982; Zlokarnik, 1980). Similar results (<1 mm bubbles and highly increased ε_G) in tall bubble columns were obtained with ethanol (Besagni et al., 2016; Jamialahmadi and Müller-Steinhagen, 1992; Oels et al., 1976; Rollbusch et al., 2015), while Krishna et al. (2000) found that the ethanol stabilizes the homogeneous flow regime (i.e. bubbly flow at higher $u_{G,S}$). In ALRs, however, organics increased ε_G up to a modest 30% (Azher et al., 2005; Kojić et al., 2015). The smaller influence of organics on ε_G in ALRs compared to BCRs was explained by, amongst others, the higher velocities of the axial liquid flow (Weiland and Onken, 1981). The expected ethanol concentration in the LanzaTech reactor (50 g.L⁻¹) (Köpke et al., 2011) is much higher than the minimum concentrations for coalescence inhibition (1–10 g.L⁻¹) (Keitel and Onken, 1982). Therefore, we can assume a low d_{32} (optimistic scenario: about 1 mm; pessimistic scenario: 3 mm) in the scenario with ethanol, whereas scale-independent d_{32} between 5 and 7 mm are observed in BCRs with air–water mixtures (Garcia-Ochoa and Gomez, 2009; Heijnen and Van't Riet (1984); Maximiano Raimundo et al., 2019). Likewise, it may be assumed that the produced ethanol could increase the local gas hold-up by at least 30% compared to solutions without ethanol.

Furthermore, temperature dependencies of the physical properties show a significant influence on the mass transfer. By operating at a temperature of 37 °C, $k_L a$ is estimated to be around 1.44 times higher than at 20 °C (Heijnen and Van't Riet (1984)), mainly due to an increased CO diffusion coefficient (+150%) and decreased liquid kinematic viscosity (-45%). However, the effect of this elevated temperature will be counteracted by a lower CO solubility through its Henry coefficient (-28%), which in turn negatively influences the MTC. The net effect of a higher temperature, however, will still be positive.

Thus, for different models describing k_L (Table 2), the impact of the bubble diameter (varied between 1 and 7 mm) and the mutual

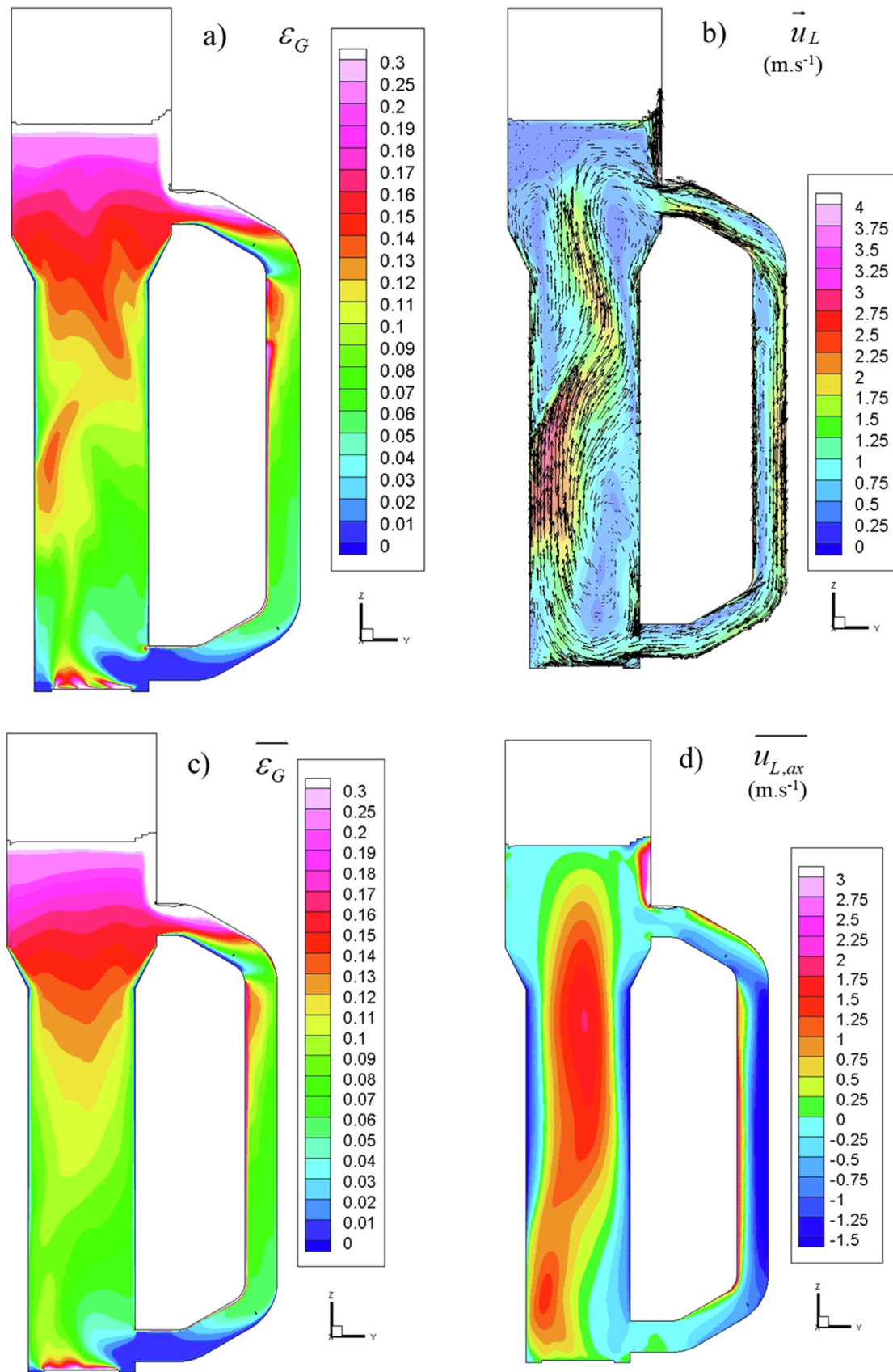


Fig. 4. Surface plots in the zy -plane ($x = 0$) of the EL-GLR ($u_{G,s} = 0.028 \text{ m.s}^{-1}$). a), b) gas hold-up and liquid velocity magnitude at a certain moment in time after establishing the flow field ($t = 1100 \text{ s}$), with arrows indicating the velocity vectors. c), d) gas hold-up and axial liquid velocity averaged over 200 s.

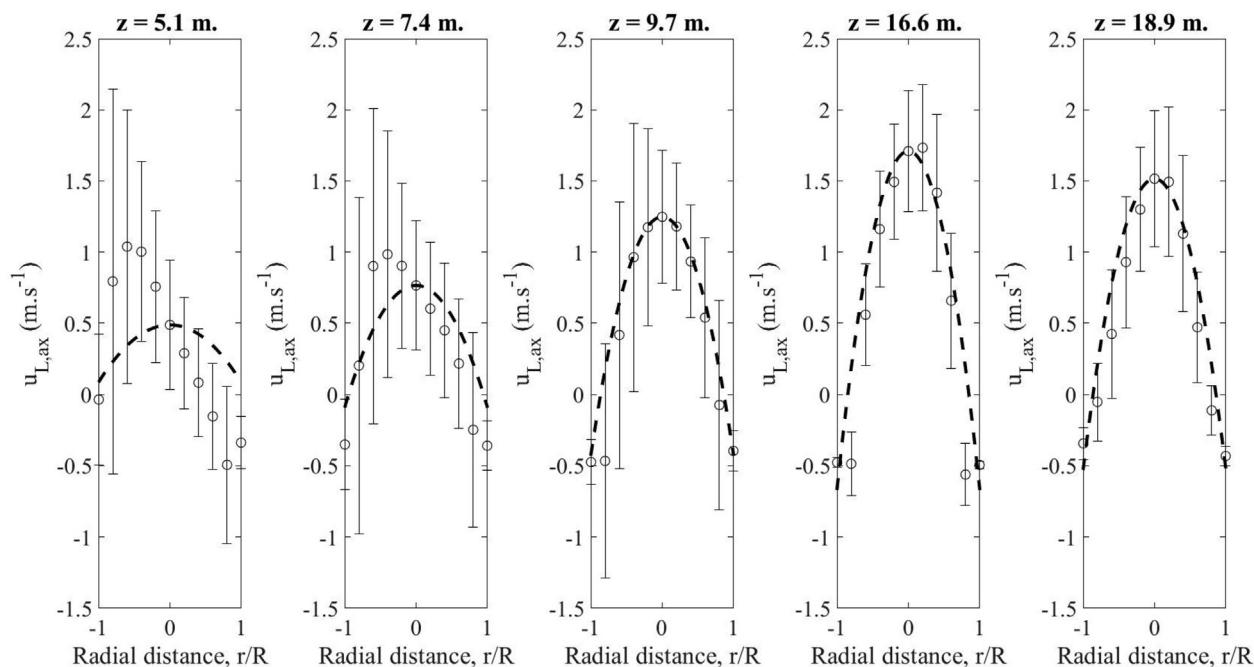


Fig. 5. Radial profiles for the axial liquid velocity in the EL-GLR ($u_{G,s} = 0.028 \text{ m.s}^{-1}$). Open circles: 200 s time-averaged mean velocities; Error bars: time-variations observed via the standard deviation; Dashed lines: parabolic profile calculated with Equation (10).

impact of increased hold-up and temperature were examined (Fig. 6). It was found that with a bubble diameter of 3 mm, most correlations predicted $k_L a$ and MTC lower than those required by the process (Figure S1), even with an increased hold-up and temperature. However, with 2 mm bubbles, sufficient $k_L a$ and MTC were predicted using the relations from Higbie (1935) and Kaštanek (1977). In addition, when including hold-up and temperature effects with 2 mm bubbles, also the relations from Calderbank and Moo-Young (1961) and Linek et al. (2005) led to adequate $k_L a$ and MTC . If the bubble diameter would be 5 to 7 mm, which is expected for air–water mixtures in industrial BCRs (Garcia-Ochoa and Gomez, 2009; Heijnen and Van't Riet, 1984), then all correlations predict insufficient $k_L a$ and MTC , causing mass transfer limitations. These values correspond with the values from

Table 1, stressing the validity of these relations in air–water dispersions.

From this sensitivity analysis we can conclude that industrial-scale syngas fermentation in the EL-GLR requires small bubble diameters ($\leq 2 \text{ mm}$), which should be obtained in combination with a high gas-hold up at 37°C . Ethanol presence promotes these conditions, while in air–water conditions (5 to 7 mm bubbles) the mass transfer limitations would not be alleviated. Therefore, our results indicate that in an industrial syngas fermentation process towards bubble-stabilizing products, e.g. ethanol, the typical mass transfer limitations that are present in air–water systems can significantly be alleviated.

It is noted that there are large differences among the $k_L a$ values predicted using the different k_L -relations. The relations based on

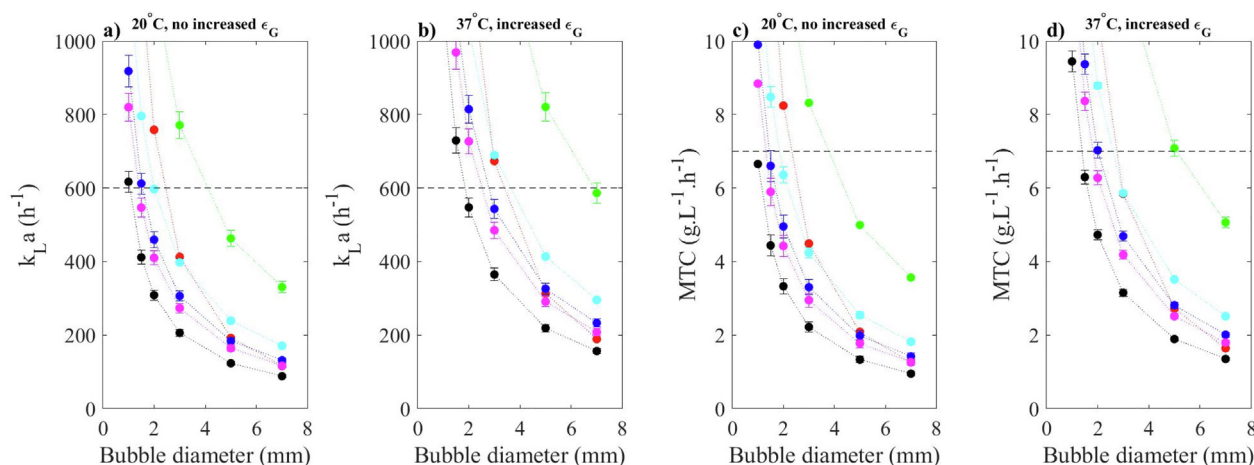


Fig. 6. $k_L a$ (a, b) and mass transfer capacity MTC (c, d), calculated using different k_L -relations (1 to 6 in Table 2) for varying bubble diameters, while considering the effect of produced ethanol on the gas hold-up and the higher temperature (b, d). Red: Higbie (1935), cyan: Calderbank and Moo-Young (1961), green: Kaštanek (1977), blue: Linek et al. (2005), magenta: Lamont and Scott (1970), black: Kawase and Moo-Young (1990), Equation 1–6 (Table 2), respectively. Error bars: standard deviation during a 200 s period with statistically stationary flow field; Black dashed line: lower value of the estimated range of the industrial process.

eddy energy dissipation rate (4–6) predict lower values than the bubble-based relations (1–2). The deviations with relations 1 and 2 could be due to underestimation of ε by the k - ε turbulence model (Gimbu et al., 2009). Accounting for this with a scaling factor, based on the overall minimum power input (Kuschel and Takors, 2020; Roels and Heijnen, 1980), would result in a 22% increase in $k_L a$. Moreover, it has been noted that relation 3 has a too high proportionality constant (Kawase and Moo-Young, 1990) compared to the similar relations 4–6. Generally, sensitivity analyses with different k_L -relations should be done in future modelling work on gas–liquid mass transfer. Experiments in EL-ALRs could determine which relation describes k_L the best in the specific reactor and how the produced ethanol and the higher temperature would influence the $k_L a$.

In some cases the $k_L a$ was predicted to be sufficient, while the MTC was not (e.g. relations 4 and 5). This indicates that the ideal-mixing assumption (Figure S1) may not hold and, instead, the local values of $k_L a$ and solubility should be taken into consideration when computing MTC . Although high $k_L a$ values were obtained at certain locations (such as in the separator), the contribution of these volumes to the overall mass transfer rate was found to be low because of the decreased CO saturation concentration (Fig. 7). However, the high $k_L a$ at the reactor top could be beneficial for CO depletion such that the off-gas only contains residual amounts of CO. As LanzaTech patented a method with the aim of, amongst others, increasing mass transfer in the headspace via a so-called ‘showerhead’ (Li et al., 2017), it is expected that these local high $k_L a$ values at the top of the reactor are indeed required for maximizing gas conversion. Although significant CO mass transfer was predicted in the downcomer, when microbial consumption takes place, only marginal transfer is expected as the relative volume of the downcomer is small and as the EL-GLR is operated in the second hydrodynamic regime.

High pressure fermentation has been mentioned as a promising strategy to increase the mass transfer rate of poorly soluble gases (Van Hecke et al., 2019). Patents indicate that in lab experiments with higher operating pressures (304 and 608 kPa) increased etha-

nol titre and productivity was obtained (Gaddy et al., 2001; Simpson et al., 2008). However, in the scientific literature, no beneficial effect was found on the productivity, while C. ljungdahlii’s product spectrum shifted from acetate and ethanol towards formate at increased pressures (Oswald et al., 2018). Inhibitory effects were observed for CO with an inhibition constant of 60 kPa (Mohammadi et al., 2014), so that increased pressures could decrease the CO consumption rate. The gas saturation concentration increases proportionally with the pressure (Equation (7)), but the gas hold-up would decrease (ideal gas law) with a constant gas (mass) flow rate. In order to study these opposing phenomena, the effect of increasing the headspace pressure on the $k_L a$ and MTC was investigated by running CFD simulations with 304 and 608 kPa headspace pressure.

It was observed that increased headspace pressures decrease the $k_L a$ significantly (Fig. 8). This is due to the decrease in gas hold-up, which decreased from 0.13 to 0.054 and 0.033, at 304 and 608 kPa respectively. Similar values of MTC at increased pressure were observed when it was calculated using the relations of Higbie (1935) and Calderbank and Moo-Young (1961), while a slight decrease was observed with the eddy-based equation. Thus, the decrease in gas hold-up was neutralized by the solubility-increase. One should note that the compressor power requirement (Van Hecke et al., 2019) increases sharply for increased headspace pressures.

At elevated pressures, one could increase the gas mass flow rate linearly with pressure to obtain a constant superficial gas velocity and thus $k_L a$, without changing the hydrodynamic regime. In our study, the mass flow rate was assumed constant at 2.11 kg.s⁻¹, causing decreasing superficial gas velocities and hold-up at elevated pressures. As it is expected that LanzaTech operates six reactors to produce in total 48 kt.a⁻¹ ethanol (Figure S1), a higher gas mass flow rate at higher pressures was not likely. If the gas flow rate would be increased proportionally with pressure (to obtain constant $k_L a$), a near-linear relationship between MTC and the compressor power requirement is obtained (Figure S4), making operating at overpressures an economical choice. Moreover, con-

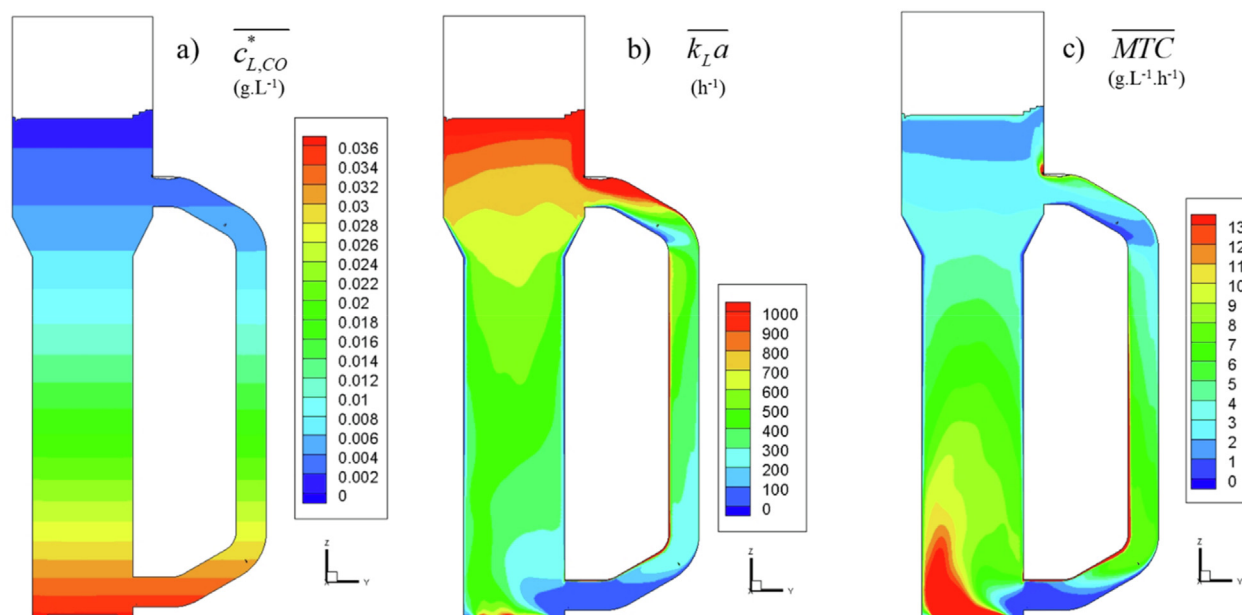


Fig. 7. Surface plots on the yz -plane of the EL-GLR ($x = 0$), showing 200 s time-averaged values for a) the CO saturation concentration in the liquid, b) the $k_L a$ as predicted using the Higbie relation (Eq. 1), c) the mass transfer capacity, assuming d_b of 3 mm, a 30% increase in gas-hold-up compared to water due to the presence of ethanol and a temperature of 37 °C.

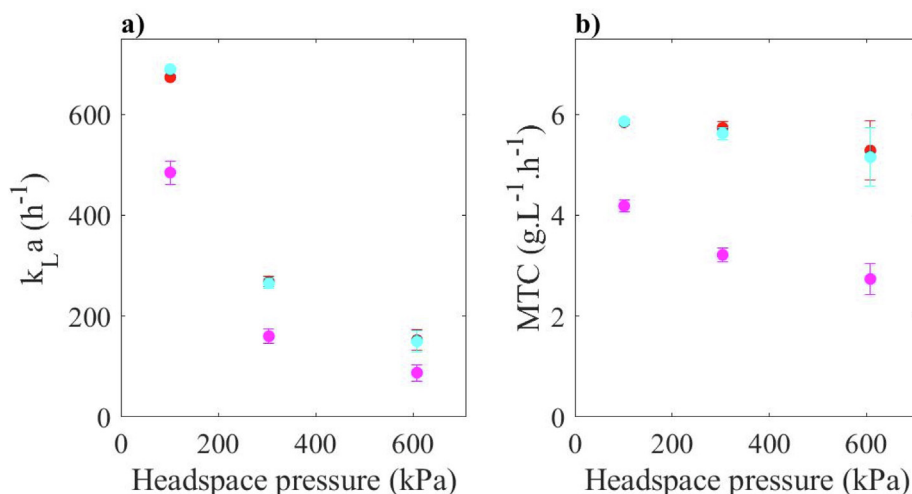


Fig. 8. Volume-average values of a) $k_L a$ and b) MTC in the EL-GLR for different headspace pressures, calculated via different k_L -relationships (Table 2) assuming d_b of 3 mm, a 30% increase in gas-hold up compared to water due to the presence of ethanol and a temperature of 37 °C. Red: Higbie (1935), blue: Calderbank and Moo-Young (1961), magenta: Lamont and Scott (1970). Bars: standard deviation during a 200 s period with statistically stationary flow field.

sidering CO-uptake kinetics, with high affinity and inhibiting effect at high dissolved CO concentrations (de Medeiros et al., 2020), we would not recommend operation at higher pressures.

3.4. Outlook

The hydrodynamics and gas-liquid mass transfer in an industrial-scale reactor for the conversion of CO-rich steel-mill off-gases by syngas fermentation were studied by computational fluid dynamics (CFD). Simulation results indicated that conditions could be reached for industrially-sufficient specific mass transfer rates ($k_L a$) and mass transfer capacities (MTC). High MTC was found possible when the operating temperature is 37 °C and by producing ethanol, which inhibits bubble coalescence to maintain relatively small bubbles ($d_b \leq 2$ mm), and increases riser gas hold-up (~30%). We recognize that other factors (e.g. particular medium components or process engineering strategies) might also be deployed to obtain such mass transfer capacities. Since most of the $k_L a$ relations from literature (Table 1) were derived in air-water systems, without considering any enhancing effects, further research is needed on the development of mass transfer correlations representing real fermentation conditions. Especially, these relations should consider the presence of bubble-stabilizing compounds such as ethanol, acetone, and acetic acid, as well as the presence of salts, antifoam agents and microbial biomass. The addition of fine particles (e.g. kieselguhr, silica) can also increase $k_L a$ substantially (Schumpe et al., 1987), possibly by minimizing bubble coalescence (Vazirizadeh et al., 2016), and could be included in such relations, which are pertinent for the development of more realistic CFD and process models.

The two-phase flow pattern in the large-scale reactor was found to be very dynamic, with large variations in the movement of a gas plume. As the local values of the gas solubility and $k_L a$ determine MTC , the high spatio-temporal resolution that can be obtained via CFD was necessary for predicting the reactor performance and for determination of the main factors influencing mass transfer. Since the main limitation of CFD is its high computational demand, further research should focus on the development of coarse-grained computational models (such as compartment models) to determine $k_L a$ and MTC in a faster way and as function of several variables such as the gas flow rate, media composition (enhancement agents), pressure and reactor scale and geometry.

The strong dynamics of the computed flow patterns in the large-scale reactor will determine the trajectories of microorganisms performing the syngas conversion. Consequently, the microorganisms would experience peaks and valleys in dissolved CO concentrations in an irregular fashion. By implementing CO-uptake kinetics, CO concentration profiles can be obtained for the different operating conditions. Euler-Lagrangian simulations can then reveal what conditions microbes experience over time ('lifelines') and how that would influence their (dynamic) behaviour (Lapin et al., 2004). Coupling the flow field with a metabolic model of *C. autoethanogenum* could reveal the influence of these dynamic conditions on the bioprocess performance and (by)product spectrum and guide the development of scale-down simulators and optimized reactor geometries (Haringa et al., 2018).

To develop an optimal bioreactor, spatial homogenization of mass transfer is imperative (Köpke et al., 2011), requiring high $k_L a$ in zones with lower solubility (e.g., separator section) and low $k_L a$ in zones with high solubility (e.g., lower riser section). Controlling the liquid flow rate in the riser, which determines the riser gas hold-up, could be done to fine-tune the local mass transfer capacity. Reducing the liquid backmixing could for example be accomplished by adding internal surfaces, such as perforated plates (Merchuk and Siegel, 1988), which would additionally promote local bubble-break up (Teli and Mathpati, 2021), or by increasing the resistance in the downcomer (Merchuk and Stein, 1981; Weiland and Onken, 1981) by decreasing its diameter or adding a pump, to force the flow at the optimal rate. By decreasing the liquid flow rate in the riser, the riser gas hold-up can be increased, possibly leading to an increased mass transfer capacity. As this may increase the mixing time (Verlaan et al., 1989c), one should balance the impact of the mass transfer time with the liquid mixing time when designing large-scale EL-GLRs. Using the downcomer, the liquid velocity and thus the gas velocity and hold-up can be adjusted, which cannot be done in a bubble column. The downcomer can also be used for product removal towards the distillation section, inflow of fresh medium or nutrients, heat transfer, and as source for supplying the showerhead (Li et al., 2017).

Alternatively, by positioning the sparger above the downcomer inlet, the gas flow could be better distributed in the riser (Chisti and Moo-Young, 1987). In this case, less bubble coalescence is expected as the gas is less likely to be pushed towards the wall opposite to the downcomer. Although the CO solubility is larger in the riser bottom, the higher sparger position would lead to a

CO-depleted zone below the sparger, which decreases the overall mass transfer capacity. CFD simulations with a sparger above the downcomer inlet confirm a 4–6% decrease in MTC, due to the low gas hold-up below the sparger (Figure S5, Table S6). Further research on the sparger position and how the downcomer (and its position) influence bubble coalescence in ethanol-rich media could be helpful for designing industrial-scale EL-GLRs with higher productivity.

In this study, all the CO transferred to the liquid phase was assumed to be instantaneously consumed by the microbes. In practice, there will be CO dissolved in the liquid phase, thus decreasing the driving force of the mass transfer. The dissolved CO concentration is determined not only by the local flow conditions and mass transfer rates, but also by the local microbial CO uptake rate, governed by the uptake kinetics (especially the affinity). The literature is very scarce on studies of CO uptake kinetics by *Clostridia* (e.g. Mohammadi et al. (2014)). Detailed CO uptake kinetics using dissolved CO concentration measurements should be developed with priority.

Many authors (Elisiário et al., 2021; Klasson et al., 1991; Yasin et al., 2015) explain the low mass transfer capacity obtained in syngas fermentation partly by the low solubility of CO. Solubility can also be affected by the ethanol fraction in the solution, and this effect has been mostly studied for O₂ dissolution. Shchukarev and Tolmacheva (1968) determined little impact of ethanol on the O₂ solubility in the water–ethanol mixture for ethanol mole fractions below 0.2. Therefore, it is not expected that the CO solubility would be affected by the produced ethanol in the studied reactor conditions (50 g.L⁻¹ ethanol or mole fraction ~ 0.02 (Köpke et al., 2011)). Since O₂ and CO have comparable Henry coefficients at 37 °C (9.6·10⁻⁶ and 8.2·10⁻⁶ mol.m⁻³.Pa⁻¹, respectively (Sander, 2015)) and the CO fraction in syngas is often higher than the O₂ fraction in air, we argue that the challenges that have to be addressed in aeration processes should be faced in syngas fermentation as well. Instead of attributing the poor performance to the solubility, research should focus on ways to enhance *k_La* in the bioreactor, e.g. by the presence of organic products.

Promising processes for the conversion of syngas towards other products, such as fatty acids (Diender et al., 2016), acetone, isopropanol and 2,3-butanediol (Köpke and Simpson, 2020) have been developed. For successful commercialization of such processes, one could benefit a lot if the produced products are mass transfer-enhancing, like ethanol, or even better.

4. Conclusion

With a CFD model, which was validated using published data from a pilot-scale reactor, we investigated the hydrodynamics of a large-scale external-loop gas-lift reactor. With this model, the gas–liquid mass transfer was studied for an industrial CO-to-ethanol fermentation process. Several relations describing the mass transfer coefficient were evaluated and *k_La* and mass transfer capacity were computed for varying process conditions.

At an operating temperature of 37 °C, with increased gas hold-up compared to air–water and smaller bubbles (≤2 mm instead of 5 to 7 mm), most available mass transfer relations predicted sufficient *k_La* and MTC for an industrially viable syngas fermentation process, in line with data published by LanzaTech. We argue that this is possible since the produced ethanol inhibits bubble coalescence, causing smaller bubbles and increased gas hold-up. This indicates that typical mass transfer limitations encountered in air–water systems can be alleviated under industrial syngas fermentation conditions.

In spite of being computationally intensive, CFD can also be used for determining high-resolution process conditions that could

not be accurately computed using simpler models. The developed hydrodynamic and mass transfer model can be used to advance research into reactor design for industrial syngas fermentation, for determination of the microbial response in such reactors using Euler-Lagrange modelling, and the development of scale-down simulators operated in a representative window.

CRediT authorship contribution statement

Lars Puiman: Conceptualization, Methodology, Investigation, Software, Formal analysis, Writing – original draft, Writing – review & editing. **Britt Abrahamson:** Conceptualization, Methodology, Software, Investigation, Formal analysis. **Rob G.J.M. van der Lans:** Conceptualization, Writing – review & editing. **Cees Haringa:** Conceptualization, Methodology, Writing – review & editing, Supervision. **Henk J. Noorman:** Conceptualization, Writing – review & editing, Supervision. **Cristian Picioreanu:** Conceptualization, Resources, Writing – review & editing, Supervision.

Declaration of Competing Interest

The authors declare that they have no known competing financial interests or personal relationships that could have appeared to influence the work reported in this paper.

Acknowledgements

This work is written as part of the MicroSynC research programme (project number P16-10/5) and is (partly) financed by the Netherlands Organization for Scientific Research (NWO).

Appendix A. Supplementary material

Supplementary data to this article can be found online at <https://doi.org/10.1016/j.ces.2022.117770>.

References

- Akita, K., Yoshida, F., 1973. Gas Holdup and Volumetric Mass Transfer Coefficient in Bubble Columns. Effects of Liquid Properties. Ind. Eng. Chem. Process Des. Dev. 12, 76–80. <https://doi.org/10.1021/i260045a015>.
- Asimakopoulos, K., Gavala, H.N., Skiadas, I.V., 2018. Reactor systems for syngas fermentation processes: A review. Chem. Eng. J. 348, 732–744. <https://doi.org/10.1016/j.cej.2018.05.003>.
- Azher, N.E., Gourich, B., Vial, C., Soulamy Bellhaj, M., Bouzidi, A., Barkaoui, M., Ziyad, M., 2005. Influence of alcohol addition on gas hold-up, liquid circulation velocity and mass transfer coefficient in a split-rectangular airlift bioreactor. Biochem. Eng. J. 23, 161–167. <https://doi.org/10.1016/j.bej.2004.12.003>.
- Bello, R.A., Robinson, C.W., Moo-Young, M., 1985. Gas holdup and overall volumetric oxygen transfer coefficient in airlift contactors. Biotechnol. Bioeng. 27, 369–381. <https://doi.org/10.1002/bit.260270323>.
- Benalcázar, A.E., Noorman, H., Maciel Filho, R., Posada, J.A., 2020. Modeling ethanol production through gas fermentation: a biothermodynamics and mass transfer-based hybrid model for microbial growth in a large-scale bubble column bioreactor. Biotechnol. Biofuels 13, 1–19. <https://doi.org/10.1186/s13068-020-01695-y>.
- Besagni, G., Inzoli, F., De Guido, G., Pellegrini, L.A., 2016. Experimental investigation on the influence of ethanol on bubble column hydrodynamics. Chem. Eng. Res. Des. 112, 1–15. <https://doi.org/10.1016/j.cherd.2016.06.009>.
- Bredwell, M.D., Srivastava, P., Worden, R.M., 1999. Reactor Design Issues for Synthesis-Gas Fermentations. Biotechnol. Prog. 15, 834–844. <https://doi.org/10.1021/bp990108m>.
- Calderbank, P.H., Moo-Young, M.B., 1961. The continuous phase heat and mass-transfer properties of dispersions. Chem. Eng. Sci. 16, 39–54. [https://doi.org/10.1016/0009-2509\(61\)87005-X](https://doi.org/10.1016/0009-2509(61)87005-X).
- Chisti, M.Y., Fujimoto, K., Moo-Young, M., 1986. Hydrodynamic and oxygen mass transfer studies in bubble columns and airlift bioreactors, in: Paper 117a Presented at AIChE Annual Meeting, Miami Beach.
- Chisti, M.Y., Moo-Young, M., 1987. Airlift Reactors: Characteristics, Applications and Design Considerations. Chem. Eng. Commun. 60, 195–242. <https://doi.org/10.1080/00986448708912017>.

- Choi, K.H., Lee, W.K., 1993. Circulation liquid velocity, gas holdup and volumetric oxygen transfer coefficient in external-loop airlift reactors. *J. Chem. Technol. Biotechnol.* 56, 51–58. <https://doi.org/10.1002/jctb.280560110>.
- Choi, K.H., Lee, W.K., 1990. Recirculation and flow structures of gas in downcomer section of a concentric cylindrical airlift reactor. *J. Chem. Technol. Biotechnol.* 48, 81–95. <https://doi.org/10.1002/jctb.280480108>.
- Cussler, E.L., 2011. *Diffusion: mass transfer in fluid systems*. Cambridge University Press, Cambridge, New York.
- de Medeiros, E.M., Noorman, H., Maciel Filho, R., Posada, J.A., 2020. Production of ethanol fuel via syngas fermentation: Optimization of economic performance and energy efficiency. *Chem. Eng. Sci.* X 5, <https://doi.org/10.1016/j.cesx.2020.100056> 100056.
- Deckwer, W.D., Burckhart, R., Zoll, G., 1974. Mixing and mass transfer in tall bubble columns. *Chem. Eng. Sci.* 29, 2177–2188. [https://doi.org/10.1016/0009-2509\(74\)80025-4](https://doi.org/10.1016/0009-2509(74)80025-4).
- Deckwer, W.D., Nguyen-Tien, K., Kelkar, B.G., Shah, Y.T., 1983. Applicability of axial dispersion model to analyze mass transfer measurements in bubble columns. *AIChE J.* 29, 915–922. <https://doi.org/10.1002/aic.690290607>.
- Dhanasekharan, K.M., Sanyal, J., Jain, A., Haidari, A., 2005. A generalized approach to model oxygen transfer in bioreactors using population balances and computational fluid dynamics. *Chem. Eng. Sci.* 60, 213–218. <https://doi.org/10.1016/j.ces.2004.07.118>.
- Diender, M., Stams, A.J.M., Sousa, D.Z., 2016. Production of medium-chain fatty acids and higher alcohols by a synthetic co-culture grown on carbon monoxide or syngas. *Biotechnol. Biofuels* 9, 1–11. <https://doi.org/10.1186/s13068-016-0495-0>.
- Elisiário, M.P., De Wever, H., Van Hecke, W., Noorman, H., Straathof, A.J.J., 2021. Membrane bioreactors for syngas permeation and fermentation. *Crit. Rev. Biotechnol.* 42 (6), 856–872. <https://doi.org/10.1080/07388551.2021.1965952>.
- Fackler, N., Heijstra, B.D., Raser, B.J., Brown, H., Martin, J., Ni, Z., Shebek, K.M., Rosin, R.R., Simpson, S.D., Tyo, K.E., Giannone, R.J., Hettich, R.L., Tschaplinski, T.J., Leang, C., Brown, S.D., Jewett, M.C., Köpke, M., 2021. Stepping on the Gas to a Circular Economy: Accelerating Development of Carbon-Negative Chemical Production from Gas Fermentation. *Annu. Rev. Chem. Biomol. Eng.* 12, 439–470. <https://doi.org/10.1146/ANNUREV-CHEMBIOENG-120120-021122>.
- Gaddy, J.L., Arora, D.K., Ko, C.-W., Phillips, J.R., Basu, R., Wikstrom, C.V., Clausen, E.C., 2001. Methods for increasing the production of ethanol from microbial fermentation. *WO2002008438A3*.
- García-Ochoa, F., Gomez, E., 2009. Bioreactor scale-up and oxygen transfer rate in microbial processes: An overview. *Biotechnol. Adv.* 27, 153–176. <https://doi.org/10.1016/j.biotechadv.2008.10.006>.
- Gimbun, J., Rielly, C.D., Nagy, Z.K., 2009. Modelling of mass transfer in gas-liquid stirred tanks agitated by Rushton turbine and CD-6 impeller: A scale-up study. *Chem. Eng. Res. Des.* 87, 437–451. <https://doi.org/10.1016/j.cherd.2008.12.017>.
- Haring, C., Tang, W., Wang, G., Deshmukh, A.T., van Winden, W.A., Chu, J., van Gulik, W.M., Heijnen, J.J., Mudde, R.F., Noorman, H.J., 2018. Computational fluid dynamics simulation of an industrial P. chrysogenum fermentation with a coupled 9-pool metabolic model: Towards rational scale-down and design optimization. *Chem. Eng. Sci.* 175, 12–24. <https://doi.org/10.1016/j.ces.2017.09.020>.
- Heijnen, J.J., Hols, J., Van Der Lans, R.G.J.M., Van Leeuwen, H.L.J.M., Mulder, A., Weltevrede, R., 1997. A simple hydrodynamic model for the liquid circulation velocity in a full-scale two- and three-phase internal airlift reactor operating in the gas recirculation regime. *Chem. Eng. Sci.* 52, 2527–2540. [https://doi.org/10.1016/S0009-2509\(97\)00070-5](https://doi.org/10.1016/S0009-2509(97)00070-5).
- Heijnen, J.J., Mulder, A., Weltevrede, R., Hols, J., van Leeuwen, H.L.J.M., 1991. Large Scale Anaerobic-Aerobic Treatment of Complex Industrial Waste Water Using Biofilm Reactors. *Water Sci. Technol.* 23, 1427–1436. <https://doi.org/10.2166/WST.1991.0595>.
- Heijnen, J.J., Van't Riet, K., 1984. Mass transfer, mixing and heat transfer phenomena in low viscosity bubble column reactors. *Chem. Eng. J.* 28 (2), B21–B42. [https://doi.org/10.1016/0300-9467\(84\)85025-X](https://doi.org/10.1016/0300-9467(84)85025-X).
- Hernández-Calderón, O.M., González-Llanes, M.D., Rios-Iribe, E.Y., Jiménez-Lam, S. A., Del Carmen Chavez-Parga, M., Escamilla-Silva, E.M., 2017. Hydrodynamics and mass transfer simulation in airlift bioreactor with settler using computational fluid dynamics. *Int. J. Chem. React. Eng.* 15. <https://doi.org/10.1515/IJCRE-2016-0173>.
- Higbie, R., 1935. The Rate of Absorption of a Pure Gas into a Still Liquid during Short Periods of Exposure. *Trans. AIChE* 31, 365–389.
- Jackson, M.L., Shen, C.-C., 1978. Aeration and mixing in deep tank fermentation systems. *AIChE J.* 24, 63–71. <https://doi.org/10.1002/AIC.690240108>.
- Jakobsen, H.A., 2014. *Bubble Column Reactors*, Chemical Reactor Modeling. Springer, Cham, Cham. 10.1007/978-3-319-05092-8_8
- Jamialahmadi, M., Müller-Steinhagen, H., 1992. Effect of alcohol, organic acid and potassium chloride concentration on bubble size, bubble rise velocity and gas hold-up in bubble columns. *Chem. Eng. J.* 50, 47–56. [https://doi.org/10.1016/0300-9467\(92\)80005-U](https://doi.org/10.1016/0300-9467(92)80005-U).
- Karcz, J., Musiał, M., Bitenc, M., Domański, M., 2013. CFD Modelling of the Fluid Flow Characteristics in an External-Loop Air-Lift Reactor. *Chem. Eng. Trans.* 32, 1435–1440. <https://doi.org/10.3303/CET1332240>.
- Kaštanek, F., 1977. The volume mass transfer coefficient in a bubble bed column. *Collect. Czechoslov. Chem. Commun.* 42, 2491–2497. <https://doi.org/10.1135/cccc19772491>.
- Kawase, Y., Halard, B., Moo-Young, M., 1987. Theoretical prediction of volumetric mass transfer coefficients in bubble columns for Newtonian and non-Newtonian fluids. *Chem. Eng. Sci.* 42, 1609–1617. [https://doi.org/10.1016/0009-2509\(87\)80165-3](https://doi.org/10.1016/0009-2509(87)80165-3).
- Kawase, Y., Hashiguchi, N., 1996. Gas - Liquid mass transfer in external-loop airlift columns with newtonian and non-newtonian fluids. *Chem. Eng. J. Biochem. Eng. J.* 62, 35–42. [https://doi.org/10.1016/0923-0467\(95\)03049-2](https://doi.org/10.1016/0923-0467(95)03049-2).
- Kawase, Y., Moo-Young, M., 1990. Mathematical models for design of bioreactors: Applications of Kolmogoroff's theory of isotropic turbulence. *Chem. Eng. J.* 43, B19–B41. [https://doi.org/10.1016/0300-9467\(90\)80048-H](https://doi.org/10.1016/0300-9467(90)80048-H).
- Keitel, G., Onken, U., 1982. THE EFFECT OF SOLUTES ON BUBBLE SIZE IN AIR-WATER DISPERSIONS. *Chem. Eng. Commun.* 17, 85–98. <https://doi.org/10.1080/00986448208911616>.
- Klasson, K.T., Ackerson, M.D., Clausen, E.C., Gaddy, J.L., 1991. Bioreactor design for synthesis gas fermentations. *Fuel* 70, 605–614. [https://doi.org/10.1016/0016-2361\(91\)90174-9](https://doi.org/10.1016/0016-2361(91)90174-9).
- Kojić, P.S., Tokić, M.S., Šijački, I.M., Lukić, N.L., Petrović, D.L., Jovičević, D.Z., Popović, S.S., 2015. Influence of the Sparger Type and Added Alcohol on the Gas Holdup of an External-Loop Airlift Reactor. *Chem. Eng. Technol.* 38, 701–708. <https://doi.org/10.1002/ceat.201400578>.
- Köpke, M., Mihalcea, C., Bromley, S.D., 2011. Fermentative production of ethanol from carbon monoxide. *Curr. Opin. Biotechnol.* 22, 320–325. <https://doi.org/10.1016/j.copbio.2011.01.005>.
- Köpke, M., Simpson, S.D., 2020. Pollution to products: recycling of 'above ground' carbon by gas fermentation. *Curr. Opin. Biotechnol.* 65, 180–189. <https://doi.org/10.1016/j.copbio.2020.02.017>.
- Krevelen, D.W., Hoftijzer, P.J., 1950. Studies on gas bubble formation - calculation of interfacial area in bubble contactors. *Chem. Eng. Prog.* 46, 19–35.
- Krishna, R., Urseanu, M.I., Dreher, A.J., 2000. Gas hold-up in bubble columns: influence of alcohol addition versus operation at elevated pressures. *Chem. Eng. Process. Process Intensif.* 39, 371–378. [https://doi.org/10.1016/S0255-2701\(00\)00093-3](https://doi.org/10.1016/S0255-2701(00)00093-3).
- Kuschel, M., Takors, R., 2020. Simulated oxygen and glucose gradients as a prerequisite for predicting industrial scale performance a priori. *Biotechnol. Bioeng.* 117, 2760–2770. <https://doi.org/10.1002/BIT.27457>.
- Laborde-Boutet, C., Larachi, F., Dromard, N., Delsart, O., Schweich, D., 2009. CFD simulation of bubble column flows: Investigations on turbulence models in RANS approach. *Chem. Eng. Sci.* 64, 4399–4413. <https://doi.org/10.1016/j.ces.2009.07.009>.
- Lamont, J.C., Scott, D.S., 1970. An eddy cell model of mass transfer into the surface of a turbulent liquid. *AIChE J.* 16, 513–519. <https://doi.org/10.1002/aic.690160403>.
- Lapin, A., Müller, D., Reuss, M., 2004. Dynamic behavior of microbial populations in stirred bioreactors simulated with Euler-Lagrange methods: Traveling along the lifelines of single cells. *Ind. Eng. Chem. Res.* 43, 4647–4656. <https://doi.org/10.1021/ie030786k>.
- Li, X., Cossey, B.J., Trevethick, S.R., 2017. Fermentation of gaseous substrates. *US9617509B2*.
- Li, X., Griffin, D., Li, X., Henson, M.A., 2019. Incorporating hydrodynamics into spatiotemporal metabolic models of bubble column gas fermentation. *Biotechnol. Bioeng.* 116, 28–40. <https://doi.org/10.1002/bit.26848>.
- Linek, V., Kordač, M., Moucha, T., 2005. Mechanism of mass transfer from bubbles in dispersions part II: Mass transfer coefficients in stirred gas-liquid reactor and bubble column. *Chem. Eng. Process. Process Intensif.* 44, 121–130. <https://doi.org/10.1016/j.ccep.2004.05.009>.
- Maximiano Raimundo, P., Cloupet, A., Cartellier, A., Beneventi, D., Augier, F., 2019. Hydrodynamics and scale-up of bubble columns in the heterogeneous regime: Comparison of bubble size, gas holdup and liquid velocity measured in 4 bubble columns from 0.15 m to 3 m in diameter. *Chem. Eng. Sci.* 198, 52–61. <https://doi.org/10.1016/j.ces.2018.12.043>.
- Menzel, T., Kantorek, H.J., Franz, K., Buchholz, R., Onken, U., 1985. Zur Strömungsstruktur in Airlift-Schlaufenreaktoren. *Chemie Ing. Tech.* 57, 139–141. <https://doi.org/10.1002/cite.330570209>.
- Merchuk, J.C., Siegel, M.H., 1988. Air-lift reactors in chemical and biological technology. *J. Chem. Technol. Biotechnol.* 41, 105–120. <https://doi.org/10.1002/jctb.280410204>.
- Merchuk, J.C., Stein, Y., 1981. Local hold-up and liquid velocity in air-lift reactors. *AIChE J.* 27, 377–388. <https://doi.org/10.1002/aic.690270307>.
- Mohammadi, M., Mohamed, A.R., Najafpour, G.D., Younesi, H., Uzir, M.H., 2014. Kinetic studies on fermentative production of biofuel from synthesis gas using clostridium ljungdahlii. *Sci. World J.* 2014, 1–8. <https://doi.org/10.1155/2014/910590>.
- Moudoud, N., Rihani, R., Bentahar, F., Legrand, J., 2018. Global hydrodynamic of hybrid external loop airlift reactor: Experiments and CFD modelling. *Chem. Eng. Process. - Process Intensif.* 129, 118–130. <https://doi.org/10.1016/j.ccep.2018.05.005>.
- Nakanoh, M., Yoshida, F., 1980. Gas Absorption by Newtonian and Non-Newtonian Liquids in a Bubble Column. *Ind. Eng. Chem. Process Des. Dev.* 19, 190–195. <https://doi.org/10.1021/i260073a033>.
- Oels, U., Schügerl, K., Todt, J., 1976. Gasanteil, Stofftransportgeschwindigkeitskoeffizient und spezifische Phasengrenzfläche in Gleichstrom-Blasensäulen. *Chemie Ing. Tech.* 48. <https://doi.org/10.1002/cite.330480121>.
- Oswald, F., Stoll, I.K., Zwick, M., Herbig, S., Sauer, J., Boukis, N., Neumann, A., 2018. Formic Acid Formation by Clostridium ljungdahlii at Elevated Pressures of Carbon Dioxide and Hydrogen. *Front. Bioeng. Biotechnol.* 6, 1–10. <https://doi.org/10.3389/FBIOE.2018.00006>.
- Reid, R.C., Prausnitz, J.M., Poling, B.E., 1987. *The properties of gases and liquids*. McGraw-Hill, New York.

- Roels, J.A., Heijnen, J.J., 1980. Power dissipation and heat production in bubble columns: Approach based on nonequilibrium thermodynamics. *Biotechnol. Bioeng.* 22, 2399–2404. <https://doi.org/10.1002/BT.260221115>.
- Rollbusch, P., Becker, M., Ludwig, M., Bieberle, A., Grünewald, M., Hampel, U., Franke, R., 2015. Experimental investigation of the influence of column scale, gas density and liquid properties on gas holdup in bubble columns. *Int. J. Multiph. Flow* 75, 88–106. <https://doi.org/10.1016/j.ijmultiphaseflow.2015.05.009>.
- Roy, S., Dhotre, M.T., Joshi, J.B., 2006. CFD simulation of flow and axial dispersion in external loop airlift reactor. *Chem. Eng. Res. Des.* 84, 677–690. <https://doi.org/10.1205/cherd.05178>.
- Sander, R., 2015. Compilation of Henry's law constants (version 4.0) for water as solvent. *Atmos. Chem. Phys.* 15, 4399–4981. <https://doi.org/10.5194/acp-15-4399-2015>.
- Schumpe, A., Saxena, A.K., Fang, L.K., 1987. Gas/liquid mass transfer in a slurry bubble column. *Chem. Eng. Sci.* 42, 1787–1796. [https://doi.org/10.1016/0009-2509\(87\)80183-5](https://doi.org/10.1016/0009-2509(87)80183-5).
- Shchukarev, S.A., Tolmacheva, T.A., 1968. Solubility of oxygen in ethanol - Water mixtures. *J. Struct. Chem.* 9 (1), 16–21. <https://doi.org/10.1007/BF00744018>.
- Siebler, F., Lapin, A., Hermann, M., Takors, R., 2019. The impact of CO gradients on C. ljungdahlii in a 125 m³ bubble column: Mass transfer, circulation time and lifeline analysis. *Chem. Eng. Sci.* 207, 410–423. <https://doi.org/10.1016/j.ces.2019.06.018>.
- Simpson, S.D., Forster, R.L.S., Rowe, M.J., Tran, P.L., Collet, C., 2008. Alcohol production process. WO2008115080A1.
- Teixeira, L.V., Moutinho, L.F., Romão-Dumaresq, A.S., 2018. Gas fermentation of C1 feedstocks: commercialization status and future prospects. *Biorefining* 12, 1103–1117. <https://doi.org/10.1002/bbb.1912>.
- Teli, S.M., Mathpati, C.S., 2021. Experimental and Numerical Study of Gas-Liquid Flow in a Sectionalized External-Loop Airlift Reactor. *Chinese Journal of Chemical Engineering* 32, 39–60. <https://doi.org/10.1016/j.cjche.2020.10.023>.
- Uchida, S., Tsuyutani, S., Seno, T., 1989. Flow regimes and mass transfer in counter-current bubble columns. *Can. J. Chem. Eng.* 67, 866–869. <https://doi.org/10.1002/cjce.5450670521>.
- Van Benthum, W.A.J., Van Den Hoogen, J.H.A., Van Der Lans, R.G.J.M., Van Loosdrecht, M.C.M., Heijnen, J.J., 1999. The biofilm airlift suspension extension reactor. Part I: Design and two-phase hydrodynamics. *Chem. Eng. Sci.* 54, 1909–1924. [https://doi.org/10.1016/S0009-2509\(99\)00034-2](https://doi.org/10.1016/S0009-2509(99)00034-2).
- Van der Lans, R.G.J.M., 1985. Hydrodynamics of a bubble column loop reactor. Delft University of Technology, Delft.
- Van Hecke, W., Bockrath, R., De Wever, H., 2019. Effects of moderately elevated pressure on gas fermentation processes. *Bioresour. Technol.* 293, 122129. <https://doi.org/10.1016/j.biortech.2019.122129>.
- Vatai, G.Y., Tekić, M.N., 1989. Gas hold-up and mass transfer in bubble columns with pseudoplastic liquids. *Chem. Eng. Sci.* 44, 2402–2407. [https://doi.org/10.1016/0009-2509\(89\)85178-4](https://doi.org/10.1016/0009-2509(89)85178-4).
- Vazirizadeh, A., Bouchard, J., Chen, Y., 2016. Effect of particles on bubble size distribution and gas hold-up in column flotation. *Int. J. Miner. Process.* 157, 163–173. <https://doi.org/10.1016/j.minpro.2016.10.005>.
- Verlaan, P., Van Eijs, A.M.M., Trammer, J., Riet, K.V., Luyben, K.C.A.M., 1989a. Estimation of axial dispersion in individual sections of an airlift-loop reactor. *Chem. Eng. Sci.* 44 (5), 1139–1146. [https://doi.org/10.1016/0009-2509\(89\)87013-7](https://doi.org/10.1016/0009-2509(89)87013-7).
- Verlaan, P., Vos, J.C., Van, T., Riet, K., 1989b. Axial dispersion and oxygen transfer in the transition from bubble column to airlift-loop reactor. *J. Chem. Technol. Biotechnol.* 45 (3), 181–190. <https://doi.org/10.1002/jctb.280450303>.
- Verlaan, P., Vos, J.C., Van, T., Riet, K., 1989c. Hydrodynamics of the flow transition from a bubble column to an airlift-loop reactor. *J. Chem. Technol. Biotechnol.* 45 (2), 109–121. <https://doi.org/10.1002/jctb.280450204>.
- Voncken, R.M., Holmes, D.B., den Hartog, H.W., 1964. Fluid flow in turbine-stirred, baffled tanks-III. Dispersion during circulation. *Chem. Eng. Sci.* 19, 209–213. [https://doi.org/10.1016/0009-2509\(64\)85031-4](https://doi.org/10.1016/0009-2509(64)85031-4).
- Weiland, P., Onken, U., 1981. Fluid dynamics and mass transfer in an airlift fermenter with external loop. *Ger. Chem. Eng.* 4, 42–50.
- Yasin, M., Jeong, Y., Park, S., Jeong, J., Lee, E.Y., Lovitt, R.W., Kim, B.H., Lee, J., Chang, I. S., 2015. Microbial synthesis gas utilization and ways to resolve kinetic and mass-transfer limitations. *Bioresour. Technol.* 177, 361–374. <https://doi.org/10.1016/j.biortech.2014.11.022>.
- Young, M.A., Carbonell, R.G., Ollis, D.F., 1991. Airlift bioreactors: Analysis of local two-phase hydrodynamics. *AIChE J.* 37, 403–428. <https://doi.org/10.1002/aic.690370311>.
- Zhang, T., Wei, C., Feng, C., Ren, Y., Wu, H., Preis, S., 2019. Advances in characteristics analysis, measurement methods and modelling of flow dynamics in airlift reactors. *Chem. Eng. Process. - Process Intensif.* 144, 107633. <https://doi.org/10.1016/j.ccep.2019.107633>.
- Ziegenhein, T., Zalucky, J., Rzehak, R., Lucas, D., 2016. On the hydrodynamics of airlift reactors, Part I: Experiments. *Chem. Eng. Sci.* 150, 54–65. <https://doi.org/10.1016/j.ces.2016.04.039>.
- Zlokarnik, M., 1980. Koaleszenzphänomene im System gasförmig/flüssig und deren Einfluß auf den O₂-Eintrag bei der biologischen Abwasserreinigung. *Korrespondenz Abwasser* 27, 728–734.
- Znad, H., Bálaš, V., Markoš, J., Kawase, Y., 2004. Modeling and simulation of airlift bioreactors. *Biochem. Eng. J.* 21, 73–81. <https://doi.org/10.1016/j.bej.2004.05.005>.
- Zuber, N., Findlay, J.A., 1965. Average volumetric concentration in two-phase flow systems. *J. Heat Transfer* 87, 453–468. <https://doi.org/10.1115/1.3689137>.